TAMPEREEN TEKNILLINEN YLIOPISTO
TAMPERE UNIVERSITY OF TECHNOLOGY

Mitra Akbari

Additive Manufacturing of Graphene for Identification and Sensing Applications

Julkaisu 1495 • Publication 1495

Tampere 2017

Tampereen teknillinen yliopisto. Julkaisu 1495
Tampere University of Technology. Publication 1495

Mitra Akbari

Additive Manufacturing of Graphene for Identification and Sensing Applications

Thesis for the degree of Doctor of Science in Technology to be presented with due permission for public examination and criticism in Sähkötalo Building, Auditorium SA203, at Tampere University of Technology, on the 6th of October 2017, at 12 noon.

Tampereen teknillinen yliopisto - Tampere University of Technology
Tampere 2017

Doctoral candidate: Mitra Akbari
Wireless Identification and Sensing Systems Research Group
The Faculty of Biomedical Sciences and Engineering
Tampere University of Technology
Finland

Supervisor: Leena Ukkonen, Prof., Dr. Tech.
Wireless Identification and Sensing Systems Research Group
The Faculty of Biomedical Sciences and Engineering
Tampere University of Technology
Finland

Instructors: Lauri Sydänheimo, Prof., Dr. Tech.
Wireless Identification and Sensing Systems Research Group
The Faculty of Biomedical Sciences and Engineering
Tampere University of Technology
Finland

Johanna Virkki, Adj. Prof., Dr. Tech.
Wireless Identification and Sensing Systems Research Group
The Faculty of Biomedical Sciences and Engineering
Tampere University of Technology
Finland

Pre-examiners: Maurizio Bozzi, Prof.
Department of Electronics
University of Pavia
Italy

Apostolos Georgiadis, Prof.
School of Engineering and Physical Sciences
Heriot-Watt University
Scotland

Opponent: Raimo Sepponen, Prof., Dr. Tech
Department of Electrical Engineering and Automation
Aalto University
Finland

ISBN 978-952-15-4006-6 (printed)
ISBN 978-952-15-4025-7 (PDF)
ISSN 1459-2045

Abstract

The huge growth of Internet of Things has been leading to a high demand in multipurpose radio frequency identification tags. The materials and manufacturing choices have subsequently become very essential for a lower cost and desired wireless performance. In addition, eco-friendly aspects are gaining more and more interest.

This thesis investigates the possibilities of novel manufacturing methods for patterning graphene-based layer on versatile substrates. Graphene is a novel nanomaterial, which has gained a huge attraction due to extraordinary mechanical and electrical properties. In this work, graphene has been introduced as a promising candidate for environmentally-friendly and cost-effective wireless platforms.

The focus of the research has been mostly on patterning and fabrication details. The used manufacturing methods are inkjet printing, doctor blade, and 3D direct writing. Additionally, required surface treatments and post treatments are investigated, which needed to be optimized according to ink and substrate materials properties. For instance, the inkjet printed graphene oxide needs annealing and a subsequent reduction process. This can be done using elevated temperature or under pulsed Xenon flashes. On the other hand, graphene inks require just one step curing process. This curing step can be carried out in a conventional oven or photonically by pulsed Xenon flashes.

The results indicate that graphene inks have a great potential for fabricating antennas and RFID tags for sensing and identification applications. In this work, the graphene passive UHF RFID tags are manufactured and characterized. Then the wireless properties are evaluated which show acceptable read range values over the UHF band. In addition, the tags show excellent reliability at high humidity and harsh bending conditions. This indicates the great potential of graphene based tags in wireless identification and sensing platforms.

Preface

This study was carried out at Wireless Identification and Sensing Systems (WISE) Research Group at Department of Electronics and Communications Engineering until end of 2016, and then at BioMediTech Institute and Faculty of Biomedical Sciences and Engineering at Tampere University of Technology (TUT) during the years 2014 – 2017. The research was funded by the Finnish Funding Agency for Technology and Innovation (TEKES) and the Academy of Finland. The work is also supported by Tekniikan Edistämissäätiö Foundation, Tuula and Yrjö Neuvo Foundation, and Elisa HPY Foundation. The financial support is gratefully acknowledged.

I would like to thank my supervisor, Prof. Leena Ukkonen, for her support and guidance throughout my work. I would also like to thank, Prof. Lauri Sydänheimo for his support during my work at WISE group. I also wish to sincerely thank my instructor, Adjunct Prof. Johanna Virkki, for her support. I would like to express my sincere gratitude to D.Sc. Jari Juuti at University of Oulu and Prof. Manos M. Tentzeris at the Georgia Institute of Technology, for their support during my visiting at Oulu and Atlanta. I would like to acknowledge all my present and past co-workers in WISE lab, and also all co-authors of publications.

I wish to thank all my friends for their support and encouragements. I would like to thank Arman for all his support, kindness and encouragement during this thesis. Most of all, I wish to think my family: my parents and my brother for their unconditional love and constant support.

Tampere, May 2017

Mitra Akbari

Contents

Abbreviation and symbols

2D	Two-Dimensional
3D	Three-Dimensional
AM	Additive Manufacturing
CS	Continuous Stream
CVD	Chemical Vapor Deposition
DB	Doctor Blade
DC	Direct Current
DI	Deionized
DOD	Drop on Demand
DPI	Drop per Inch
DW	Direct Writing
GNP	Graphene Nanoplatelets
GO	Graphene Oxide
HF	High Frequency
HV	High-Voltage
IC	Integrated Circuit
ID	Identification
IoT	Internet of Things
IR	Infra-Red
LF	Low Frequency
NFC	Near Field Communication
R2R	Roll to Roll
RF	Radio Frequency
RFID	Radio Frequency Identification
RGO	Reduced Graphene Oxide
RH	Relative Humidity
SLGO	Single Layer Graphene Oxide
TFT	Thin-Film Transistors
UHF	Ultra-High Frequency
UV	Ultra-Violet

List of publications

I Akbari, M., Sydänheimo, L., Juuti, J., Vuorinen, J. and Ukkonen, L., "Characterization of Graphene-Based Inkjet Printed Samples on Flexible Substrate for Wireless Sensing Applications," *2014 IEEE RFID Technology and Applications Conference (RFID-TA)*, Tampere, 2014, pp. 135-139.

II Akbari, M., Sydänheimo, L., Juuti, J. and Ukkonen, L., "Flash Reduction of Inkjet Printed Graphene Oxide on Flexible Substrates for Electronic Applications," *2015 IEEE 15th International Conference on Nanotechnology (IEEE-NANO)*, Rome, 2015, pp. 93-96.

III Akbari, M., Khan, M. W. A., Hasani, M., Björninen, T., Sydänheimo, L. and Ukkonen, L., "Fabrication and Characterization of Graphene Antenna for Low-Cost and Environmentally Friendly RFID Tags," *IEEE Antennas and Wireless Propagation Letters*, vol 15, pp. 1569 – 1572, 2016.

IV Akbari, M., Virkki, J., Khan, M. W. A., Sydänheimo, L. and Ukkonen, L., "Towards Eco-Friendly and Cost-Effective Passive RFID Applications," *2016 10th European Conference on Antennas and Propagation (EuCAP)*, Davos, 2016, pp. 1 – 4.

V Akbari, M., Sydänheimo, L., Rahmat-Sami, Y., Virkki, J. and Ukkonen, L., "Implementation and Performance Evaluation of Graphene-Based Passive UHF RFID Textile Tags," *2016 URSI International Symposium on Electromagnetic Theory (EMTS)*, Espoo, 2016, pp. 447-449.

VI Akbari, M., Virkki, J., Sydänheimo, L. and Ukkonen, L., "Toward Graphene-Based Passive UHF RFID Textile Tags: A Reliability Study," *IEEE Transactions on Device and Materials Reliability*, vol 16, no. 3, pp. 429 – 431, 2016.

VII Akbari, M., Virkki, J., Sydänheimo, L. and Ukkonen, L., "The Possibilities of Graphene-Based Passive RFID Tags in High Humidity Conditions," *2016 IEEE International Symposium on Antennas and Propagation (APSURSI)*, Fajardo, 2016, pp. 1269 – 1270.

VIII Akbari, M., He, H., Juuti, J., Tentzeris, M. M., Virkki, J. and Ukkonen, L., "3D Printed and Photonically Cured Graphene UHF RFID Tags on Textile, Wood, and Cardboard Substrates," *International Journal of Antennas and Propagation*, vol 2017, Article ID 7327398, 2017.

1 Introduction

The Internet of Things (IoT) enables people, devices and things to connect and communicate with themselves and the environment. The IoT has been vastly developing as an integrated part of future life, allowing embedded ubiquitous electronics to turn everyday objects into "smart" things, and interconnecting them with extended Internet technologies. The applications of the IoT have been rapidly growing, and emerged beyond imagination, along with essential supporting components, e.g., sensors, actuators, and radio-frequency identification (RFID) tags. (Miorandi et al. (2012)) In particular, passive ultra-high frequency (UHF) RFID tags can enable and increase the IoT applications for wireless identification and sensing purposes. Beside the design of these RFID tags, manufacturing methods and materials play an important role on the resulting wireless performance along with the final costs.

Recent progresses in additive manufacturing (AM) techniques open new horizon in using widespread choices of materials in the electronic industry, specially in wearable electronics and RFID technology. The AM technologies enable to utilize various kind of substrates and novel functional materials. Additionally, AM methods provide the decrease in manufacturing steps and reduce in material use, leading to a lower price of RFID tags along with environmentally-friendly aspects.

In RFID components, metallic materials are commonly used as main conductive materials. Recently, the manufacturing of eco-friendly and cost-effective RFID tags has been gained extensive attention along with their reliability and mechanical durability in different environments. One possibility is to replace metallic materials by carbon-based nanomaterials e.g., graphene. The graphene has great potential due to providing low processing temperature, as well as chemically stable, mechanically flexible, and light weight compared to metals. (Huang et al. (2015))

1.1 Aim and scope

The aim of this work is to use novel manufacturing methods for patterning graphene on versatile substrates. *3D direct writing, doctor blade, and inkjet printing* are used to print graphene-based inks on flexible polymeric surfaces and green substrates e.g. paper, cardboard, and plywood. The main focus of this thesis is to manufacture maintenance-free *graphene-based passive UHF RFID tags* integrated within different eco-friendly components and structures.

The performance of graphene-based RFID tags presented in this thesis are evaluated through wireless tag measurements. Beside wireless performance, the tags are studied based on material and electrical characterizations.

The read range of graphene passive RFID tags changed as subjected to mechanical and humidity changes. Moreover, these tags show acceptable reliability and durability in high humidity conditions and harsh bending situations. This indicates the potential of graphene based passive UHF tags to act as a sensor for environmental and mechanical changes.

Using novel materials, such as graphene, has been ongoing new research and it needs more investigation on ink development, fabrication methods, and also post-treatment process. In this thesis, the wireless performance of graphene passive UHF RFID tags has been enhanced by integrating of 3D printing with photonic curing. The photonic curing is known as a fast and economical process assisting rapid production together with additive manufacturing methods. Based on extensive study in this thesis, graphene passive UHF RFID tags also have great potential market in the fields of wearable electronics.

1.2 Structure of the thesis

This thesis outlines the work done in eight publications, and is divided into five chapters. The structure of thesis is shown in Figure 1.1. Chapter 1 is a brief introduction about the aim, results, and structure of thesis, followed by author's contributions. Chapter 2 presents the background study about carbon-based nanomaterials, RFID technology, followed by different manufacturing methods and required post-treatments. Chapter 3 presents the materials and methods, which are utilized in this study. The properties of utilized materials and printing techniques are extensively explained. Chapter 4 is devoted to the results and discussion, including material, electrical, and wireless characterizations of fabricated samples. Chapter 5 summarizes the work, and presents final conclusion, and future trends.

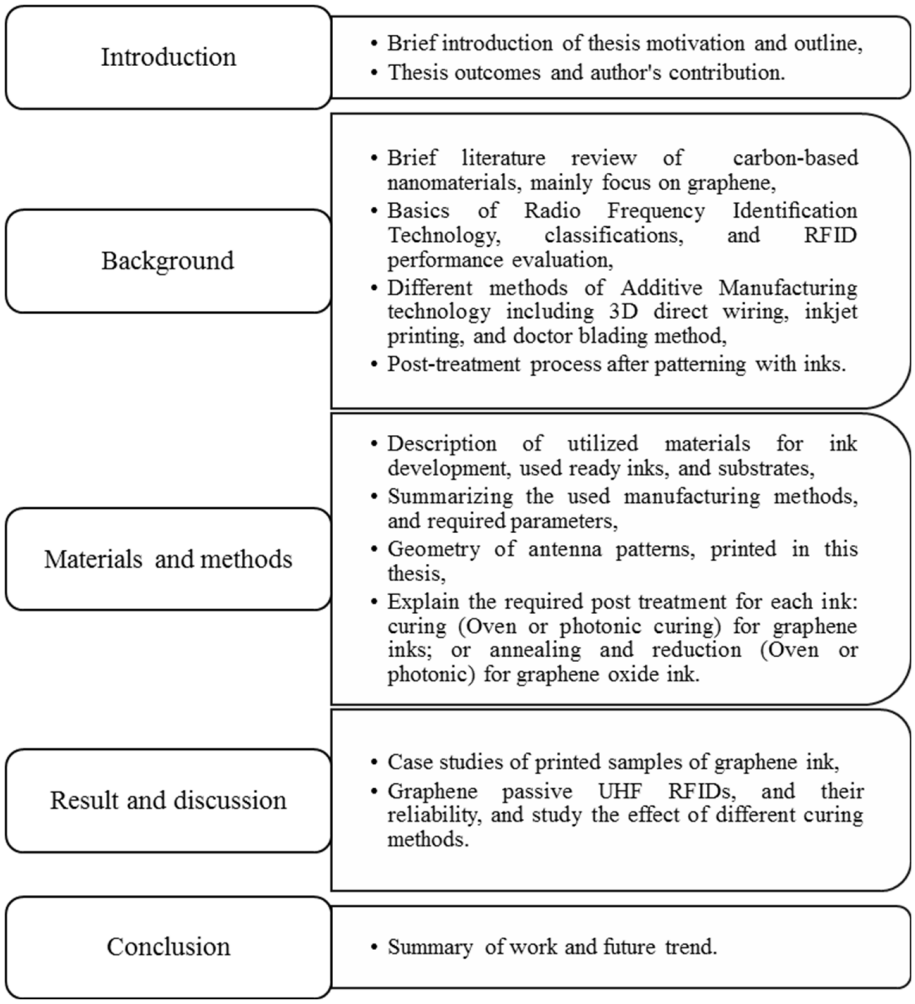

Figure 1.1: Structure of the thesis.

1.3 Author's contribution

This thesis includes scientific outputs followed by eight publications. These publications are the result of collaboration. The contribution of author is presented as follows:

Publication I, The author was the main contributor to this paper including: ink development, pre-treatment process, fabrication and post-treatments. The material and electrical characterization tests were carried out by author and J. Juuti together at University of Oulu. The manuscript was written by author and revised with the co-authors.

Publication II, The author was the main contributor to this paper, including all fabrication steps and ink development. The author and J. Juuti characterized printed samples at University of Oulu. The author wrote the manuscript. The manuscript was revised and improved with the co-authors.

Publication III, The author was the main contributor to this paper. The authors

designed and fabricated the antennas. The material characterization was carried out by author. The wireless performance of dipole antenna was measured with the help of M. Hasani. The wireless performance measurement of the fabricated RFID tag and the simulations were performed with the help of M. W. A. Khan. The author wrote the manuscript except for the paragraphs related to principles of RF measurements. The manuscript was revised and improved with the co-authors.

Publication IV, This paper continues the work presented in **Publication III**. The author was the main contributor to this paper. The author fabricated graphene-based passive UHF RFID on cardboard. The author did the material and electrical characterization. RF properties were measured with the help of J. Virkki. The author and J. Virkki analyzed and compared wireless performance of graphene tag with with the results of metallic passive UHF RFIDs. The author wrote the manuscript. The manuscript was revised and improved with the co-authors.

Publication V, The author was the main contributor to this paper. The author fabricated passive RFID tags and did the characterisation processes. RF properties were measured with the help of J. Virkki. The author and J. Virkki analyzed the measurements and characterizations. The author wrote the manuscript and the manuscript was revised and improved with the co-authors.

Publication VI, The author was the main contributor to this paper. The author primarily planned, fabricated, and characterized the printed samples. Wireless measurements were carried out with the help of J. Virkki. The author and J. Virkki carried out the reliability tests and analyzed the measurements and characterizations. The author wrote the manuscript and the manuscript was revised and improved with the co-authors.

Publication VII, The author was the main contributor to this paper. The author manufactured the samples and characterized the printed sample. Wireless properties were measured with the help of J. Virkki. The author and J. Virkki did the reliability experiments, and then analyzed the measurements and characterizations. The author wrote the manuscript and the manuscript was revised and improved with the co-authors.

Publication VIII, The author was the main contributor to this paper. The author primarily planned this paper and carried out all fabrication steps. H. He measured wireless properties. The author wrote the manuscript. The manuscript was revised and improved with the co-authors.

2 Background

2.1 Carbon-based nanomaterials

Carbon has variety of structural forms as a result of its special electron configuration with the other carbon atoms or other elements. Until 1964, only two carbon allotropes have been known as diamond with sp^3-hybridized and graphite with sp^2-hybridized carbon lattices.

During last decades, various allotropes of carbon-based nanomaterials have been introduced. All Carbon nanomaterials are composed entirely of sp^2 bonded graphitic carbon. As it is illustrated in Figure 2.1, two-dimentional graphene is one layer of graphite which is a basis of all further new carbon allotropes such as fullerenes (zero-dimensional) and carbon nanotubes (CNTs) (one-dimensional). (Gebhardt (2012); Jariwala et al. (2013); Schäffel (2013))

The properties of carbon nanomaterials mainly depend on their atomic structures and also interactions with other materials. In general, they show remarkable thermal, mechanical, and chemical properties. (Gebhardt (2012); Jariwala et al. (2013))

2.1.1 Graphene

Graphene has been studied theoretically as graphitic materials, and single graphene layers had been considered as thermodynamically unstable material. In 2004, A. Geim's group discovered single graphene layers with unique atomic structure and the extraordinary electronic properties. (Molitor et al. (2011); Schedin et al. (2007))

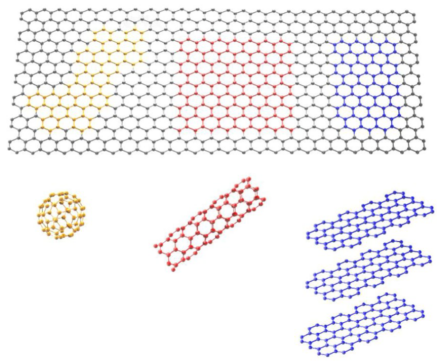

Figure 2.1: Different allotropes of carbon which are composed by graphene layer: fullerenes (orange), carbon nanotubes (red) and graphite (blue) can be constructed. (Gebhardt (2012))

Graphene is a two-dimensional (2D) nanomaterial with planer honeycomb structure (Figure 2.2). It consists of three carbon electrons with in-plane strong covalent sp^2 bonds with high binding energy (615 kJ/mol). The forth inter-plane electron is above or below this honeycomb plane having extremely lower binding energy. This plays an important role in graphene multi-layers interaction to each other or other particles. (Larciprete et al. (2011)) The interplaner space of graphene has been measured as 0.335 nanometers. In addition, the length of carbon bonds in graphene plane is approximately 0.142 nanometers. (Heyrovska (2008); Schäffel (2013))

The unique atomic structure of graphene leads to many extraordinary properties. The huge interest in graphene is extensively as a result of its electronic properties. Graphene shows high charge mobility about $200,000\ cm^2V^{-1}s^{-1}$. (Shen et al. (2012))

Both monolayer and bilayer graphene have a zero band gap. Thus, it is expected that few layers of graphene behave as metals. Based on recent research, bilayer graphene shows a band-gap by applying electric displacement field. Thus, bilayer graphene behaves as a semiconductor in this case. (Savage (2009))

Due to the strong covalent bonds, pristine graphene has high mechanical strength (Young's modulus of $1100\ GPa$). Graphene also has high surface area ($2630\ m^2/g$) and high thermal conductivity ($5000\ Wm^{-1}K^{-1}$). (Shen et al. (2012), **Publication I**)

Furthermore, graphene has intrinsic biocompatibility which makes it suitable candidate for biomedical applications from biological sensing, bioimaging to antibacterial materials and drug delivery. (Shen et al. (2012); Zhang et al. (2016))

The most common way to produce graphene is thermally reducing of graphene oxide (GO). This is a cost-effective method for mass production. (Larciprete et al. (2011)) Graphene oxide has a layered structure similar to graphene including oxygen containing groups. These oxygen groups increase the interlayer distance resulting hydrophilic layers. By reduction process, those oxygen containing groups are removed from GO and changed into graphene like structure which called reduced graphene oxide (RGO).

Recently, intensive work has been done on patterning of graphene for electronic devices. It has great potential utilizing in various applications and industries such as gas sensors, supercapacitors, solar cells, and etc. The result properties and final application play a significant role in choosing of fabrication method.

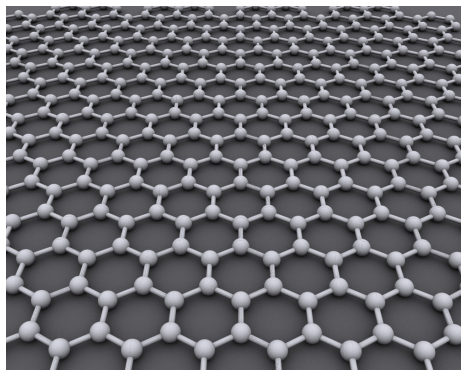

Figure 2.2: Schematic atomic structure of single layer graphene. (AlexanderAIUS (2014))

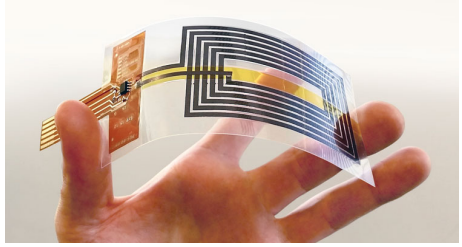

Figure 2.3: Fully flexible graphene-based NFC antennas. (Graphene-flagship (2016))

The pattering of graphene can be carried out via several methods such as chemical vapor deposition (CVD), epitaxial growth, and lithography (Feng et al. (2012)). Recently, different additive manufacturing methods have gained significant attraction offering cost-effective, flexible, and rapid patterning of graphene for various applications. For instance, Le et el. fabricated graphene-based supercapacitors by inkjet printer (Le et al. (2011)). Furthermore, there are several researches on utilizing different printing methods to fabricate graphene-based sensors for environmental monitoring. The examples include gas, temperature and humidity sensors. (Andò et al. (2015); Kang et al. (2015); Vuorinen et al. (2016)) The additive manufacturing techniques are explained in details in Section 2.3.

Integrating of graphene with its unique properties with novel manufacturing methods opens new horizon to radio-frequency (RF) electronics, wearable electronics and Internet of Things (IoT). (Palacios et al. (2010), **Publication IV**)

Huge potential lies in implementing graphene as antenna material. Graphene brings environmental-friendly aspects, flexibility in design change, lighter weight, and lower cost compared to typically-used metallic materials. Additionally, graphene components require typically low-processing temperature. Therefore, graphene makes an excellent choice for future wireless applications.

Several preliminary researches have been focused on implementing additive manufacturing techniques for graphene-based RFID antennas. The example is screen printing of graphene ink, and subsequently subjected to rolling compression to form binder-free graphene layer. This leads to improve the conductivity and antenna performance. (Huang et al. (2015)) Moreover, researchers recently fabricated fully flexible graphene Near-Field-Communication (NFC) antenna (see in Figure 2.3). This can be used in future applications such as wearable NFC tag interacting with other devices. (Graphene-flagship (2016))

2.2 Radio frequency identification technology

Radio Frequency Identification (RFID) is a wireless automatic identification technology using electromagnetic interaction to identify and track people or objects equipped with transponders or tags.

The basic components of RFID system is shown in Figure 2.4. The RFID system is typically comprised of RFID device, tag reader with an antenna and transceiver, and computer. The tags are composed of an antenna and an RFID integrate circuit (IC). The tags come in wide variety of shapes and sizes, fabricated on different substrates with different conductive materials. Several tag prototypes are shown in Figure 2.5. In this work, the antenna is manufactured on a substrate, and different manufacturing methods can be used which will be explained in details in Section 2.3 and Section 3.3.

The reader sends and receives information communicating with tag. The reader sends these data to a computer which known as data processing system. This computer is usually an interface between RF system and application layer.

Furthermore, RFID technology also provides the simultaneous identification of several objects. The RFID technology has many applications in our daily life. For instance, it has been used in access control systems such as in keyless employee identification cards, entrance of automatic toll collection, animal tracking, bracelet for infant ID and security. (Hunt et al. (2007))

The intensive researches have been carried out on RFID technology to improve RFID systems, lower the costs, and improve reliability of RFID tags. The RFID applications are vastly growing and are incorporated into a wide range of industries. The significant advantageous of RFID tags is the possibility of embedding them in different products. (Hunt et al. (2007))

Due to target application, the antenna and chips can be protected from environmental conditions by different protective housings. These encapsulation techniques keep the tags' integrity and boost their lifetime, accuracy and reliability. For instance, the tags can be encapsulated in a small glass or a plastic layer which laminated on top of product's surface. (Dobkin (2008); Sipilä (2016); Want (2006))

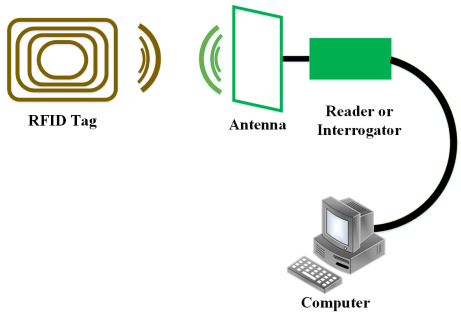

Figure 2.4: Schematic basics of typical RFID system.

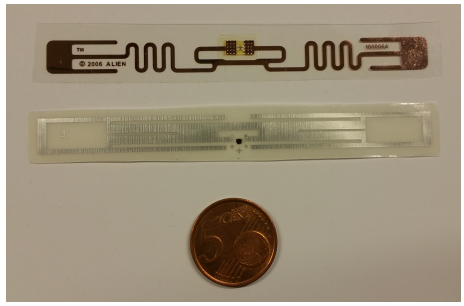

Figure 2.5: Flexible RFID tag prototypes. Upper tag: copper UHF tag on transparent substrate. Lower tag: silver UHF tag on a transparent adhesive substrate.

Table 2.1: Different Frequency ranges and their RFID applications. (Dobkin (2008); Hunt et al. (2007); Popov et al. (2008); Sipilä (2016))

Frequency band	Read ranges	Characterization	Applications
LF (125-134 kHz)	Up to 2 m Typically 30 cm	Vulnerable to interface from other radio systems Relatively low data rate Generally passive	Keyless entry Car immobilizer
HF (13.56 kHz)	≈ 1 m	Proper to use in Liquid medium Medium data rate Generally passive	Pharmaceutical supply chain
UHF (860-960 MHz)	Up to 14 m for active tags, Average 3-5 m for passive tags	Generally active but passive also High data rate Very poor performance near metal and water	Toll collection systems Baggage handling
Microwave (2.5 GHz and up)	Typically 1 m	Generally active but also passive Very high data rate Very poor performance near metal and water	Railway vehicle monitoring Toll collection systems

2.2.1 RFID classifications

Depending on tags energy sources and power supply, the RFID system can be categorized into active, semi-passive, and fully passive. Active tags have internal energy source such as a battery. This on-board power source is used when the tag needs to transmit data to the interrogator. This provides an opportunity for active tags to communicate with less powerful interrogators and ability to transmit data to longer ranges up to several hundred meters. (Dobkin (2008); Hunt et al. (2007))

Fully passive RFID tags have no internal power source, and they just derive power from the interrogator's signal and excite itself to transmit data. The passive tags have less complex structure, typically smaller, lighter, and less expensive compared to active tags. They don't require batteries or maintenance. Due to unlimited life and small size, passive RFID tags have a great potential to fit into a practical adhesive label. However, the effective ranges are much shorter compared to active tags. (Dobkin (2008); Want (2006))

The semi-passive tags have internal power source for their operation but they derive power from interrogator for device communication. The semi-passive tags have properties between active and passive tags. (Dobkin (2008); Sipilä (2016))

The RFID systems can be also classified based on the utilized frequency ranges into three groups: low-frequency (LF), high-frequency (HF), and ultra-high-frequency (UHF). The frequency ranges of each group and their RFID applications are mentioned in Table 2.1.

In general, the effective ranges for low-frequency passive tags are around 30 cm, HF passive tags cover approximately 1 m, and UHF passive tags typically have ranges about 3-5 m. (Dobkin (2008)) Due to relatively long wavelength of HF signals, they likely penetrate into water compared to UHF and microwave signals. Thus, HF tags are suitable for tracking liquid containers. Metals are electromagnetic reflectors and they can have affects on the system operation, and these affects are getting worse in higher frequencies. (Hunt et al. (2007)) The focus of this thesis is on passive UHF RFID.

2.2.2 RFID measurements

Based on RFID system, different parameters can be measured either in normal room condition or inside RFID measurement cabinet which is an anechoic chamber preventing interfering of environmental issues on the measurement. This provides reliable measurements to compare results to each other. The most common measurements of antenna parameters are read range values and antenna radiation patterns including antenna's directivity, gain and efficiency, the impedance, and polarization. (Derbek et al. (2007); Sipilä (2016))

Based on physic laws, electromagnetic waves can be radiated in all conductors with carrying voltage and/or current. In antennas, these radiation or reception of electromagnetic waves are optimized for specific frequencies. This optimization occurs due to tunning of design parameters. The antenna performance can be exactly predicted regarding mathematical calculations. (Finkenzeller (2003))

The read range value i.e. the reading distance is one of the significant measurements which can be used to evaluate the performance of RFID tags. In this study, Voyantic Tagformance lite UHF RFID measurement system, which is the most widely used tool for verifying tag design, selecting tags for a specific use case, was used for evaluating the fabricated tags. (Voyantic (2017)) This system contains an RFID reader with an adjustable transmission frequency in the range of 0.8 to 1 GHz, and output power up to 30 dBm, and it has ability to provide the recording of the backscattered signal strength (down to -80 dBm) from the tag under test.

The tags were evaluated for their wireless performance by recording the smallest output power of the reader (known as threshold power), at which a valid 16-bit random number from the tag was received as a response to the query command in ISO 18000-6C communication standard. Firstly, the wireless channel from the reader antenna to the tag measurement location was characterized with a reference tag. The theoretical read range of the measured tag was then calculated based on the measured path loss and threshold power, and it is based on the relationship given in Equation 2.1, which is explained in details in reference (Virkki et al. (2015)).

$$d_{Tag} = \frac{\lambda}{4\pi}\sqrt{\frac{EIRP}{P_{TS}L_{fwd}}} \tag{2.1}$$

where λ is the wavelength transmitted from the reader antenna, P_{TS} is the measured threshold power, L_{fwd} is known as forward losses, and EIRP is the emission limit of an RFID reader, given as equivalent isotropic radiated power. Here EIRP = 3.28 W, which is the emission limit in European countries.

2.3 Additive manufacturing technology

The additive manufacturing (AM) technology refers to basically integrating materials layer by layer. In general, using AM technology leads to reduction of required resources. The AM technology is also known as rapid prototyping. This speeding up is related to fast manufacturing of components, using computer throughout which leads to reduction in numbers of process steps. Both decrease in material use and process steps lead to cost-effective technology. The other important benefit of AM machines is their accuracy

which generally provides high resolution structures with ranges of few microns. (Gibson et al. (2015))

Additive manufacturing techniques provide patterning with wide range of materials. For instance, polymers with wide range of mechanical properties can be pattered by both 2D and 3D manufacturing methods. (Gibson et al. (2015))

Furthermore, direct printing technology enables 3D structures of ceramic suspensions such as alumina, and zirconia based structures. The most researches on printing metals are related to electronic applications. For instance, solder material is the best option for printing regarding low melting point. In addition, most recently extensive research has been focused on 3D fabrication of metallic structures such as copper, aluminum, and various solders. (Gibson et al. (2015))

The most significant application of printable technologies is in printable electronics. The printing technologies such as inkjet printing and 3D printing are mold-free technologies along with low consumed materials; they provide cost-effective and rapid manufacturing process.

2.3.1 Direct writing technologies

Direct writing (DW) means any technology that has ability to generate 2D or 3D structures on any kinds of flexible or rigid surfaces with planer or conformal complex geometry. The DW technologies require no masks or tooling. (Gibson et al. (2015); Lewis and Gratson (2004); Mortara et al. (2009))

The most common structures using DW technologies are in passive or active electronic components such as conductors, insulators, antennas, batteries, etc. In the additive manufacturing community, definition of DW typically consists of manufacturing technologies to write or print structures or electronics directly from a computer file with feature resolution below 50 μm. (Gibson et al. (2015))

DW methods can be categorized into five groups, including ink-based, laser transfer, thermal spray, beam deposition, liquid-phase, and beam tracing methods. Most of these methods are using devices equipped with a 3D programmable dispensing or deposition head to accurately apply small amounts of material on flat or conformal complex geometries. The ink-based DW technology is explained in details and used in this work. More details about other DW methods can be found in reference (Gibson et al. (2015)).

Ink-based direct writing

The most simple and cost-effective DW process involves using of widespread liquid inks. The versatile types of inks can be used including colloid, nanoparticles, organic-based, or sol-gel. (Gibson et al. (2015); Lewis and Gratson (2004))

These inks solidify after deposition depending on the ink via evaporation, gelation, solvent-driven reactions, or thermal energy. The result deposited layer is left with desired properties.

DW inks can be deposited as droplets by using a printing head or extruding of a continuous filament through a nozzle (see in Figure 2.6). (Gibson et al. (2015); Lewis (2002))

The rheological properties of DW inks play an important role on the patterning process. The inks must flow through nozzles, keep the a constant and controllable shape after deposition, and also have the ability to fill the small gaps or voids. (Gibson et al. (2015))

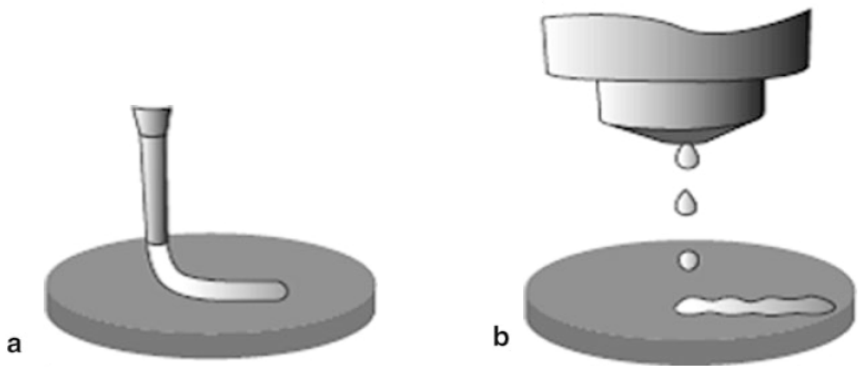

Figure 2.6: Schematic drawing of ink-based direct writing techniques: (a) continuous writing, and (b) jetting of droplets. (Gibson et al. (2015); Li et al. (2007))

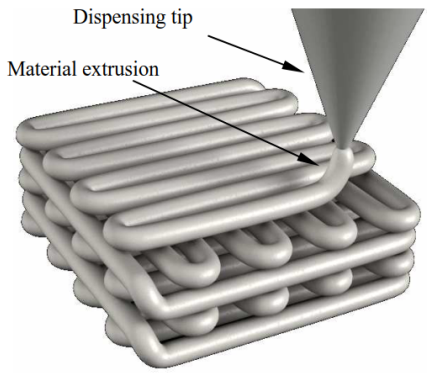

Figure 2.7: Schematic illustration of direct writing. (Gibson et al. (2015); Li et al. (2007))

2.3.2 Nozzle dispensing processes

In nozzle dispensing processes, a pump or syringe mechanism are used to push ink into the nozzle. These nozzle of DW systems are generally equipped with X-Y-Z motion control system and a scanning system. First the topography of surfaces with 3D complex geometries are scanned and then the inks are deposited. The motion control system enhances the printing accuracy and reliability. This enables to print complex structures on uneven surfaces. The example of printing scaffolds is shown in Figure 2.7.

The nozzle design plays an important role in regulating the shape and size of the deposited material. It determines the printing resolution and the types of used ink. The pump design is also significant factor controlling volume and repeatability of dispensing flow, the precise "start and stop" of flow, and the deposition speed.

The wide spread variety of inks can be used in nozzle direct writing system such as solders, metallic or ceramic based inks, adhesives and epoxies. The example applications are to manufacture scaffolds and microfluidic networks. (Gibson et al. (2015); Lewis and Gratson (2004); Therriault et al. (2003))

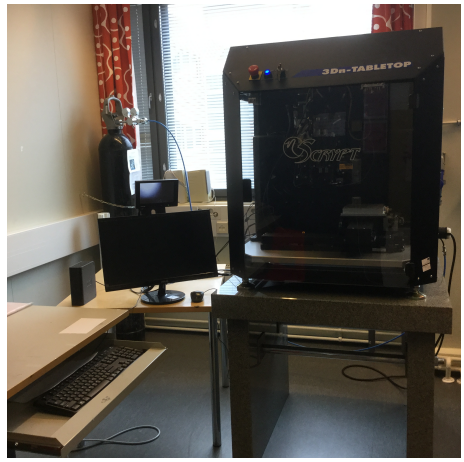

Figure 2.8: The nScrypt tabletop series 3Dn equipped with micro-dispensing system.

In this work, nScrypt DW system (Figure 2.8) is used, which equipped with an extrusion nozzle and deposition systems. The details are explained thoroughly in Section 3.3.1.

2.3.3 Inkjet printing

Inkjet printing is a flexible technology, which can provide films with thin to intermediate thickness with high printing resolution. There is no need for physical masks or stencils and the pattern can be drawn or changed easily on the digital control file. This leads to rapid manufacturing which is a remarkable benefit. In addition, inkjet printing is a contactless manufacturing process. It means printing is carried out without physical contact between ink deposition head and substrate. (Niittynen (2015))

The inkjet printers are facilitated with actuators, assisting to the movement of inkjet heads, consequently, the droplets are formed and jetted through nozzles and deposited on to the substrates. (Gibson et al. (2015))

In general, inkjet printers are categorized into either continuous stream (CS) or drop on demand (DOD) mode. In continuous mode, the ink is pumped into nozzles as a continuous column of liquid by applying a steady pressure to the ink container. (Gibson et al. (2015))

In DOD mode, the ink exits through nozzles as discrete droplets. The droplets are formed by pressure pulses in the nozzle. These pressure pulses are formed by actuators (see in Figure 2.9). There are three main energy sources for actuators: heat, piezoelectric deflection, and electric field. The principle of DOD piezoelectric actuators and droplet formation are illustrated in Figure 2.10.

In this work, Fujifilm Dimatix-2831 (DMP-2831) inkjet printer was used, which is a pizoelectric DOD inkjet printer. In Figure 2.11, the inkjet printer and a cartridge filled by ink are shown. The cartridge head has 16 nozzles with 10 picoliter drop volume.

During inkjet printing, the first challenge is droplet formation. The droplet forming behavior can dramatically change due to small changes in materials or other setup parameters. The viscosity plays an important role in droplet creation and materials jetting. For droplet creation, the maximum viscosity of ink is generally in the range

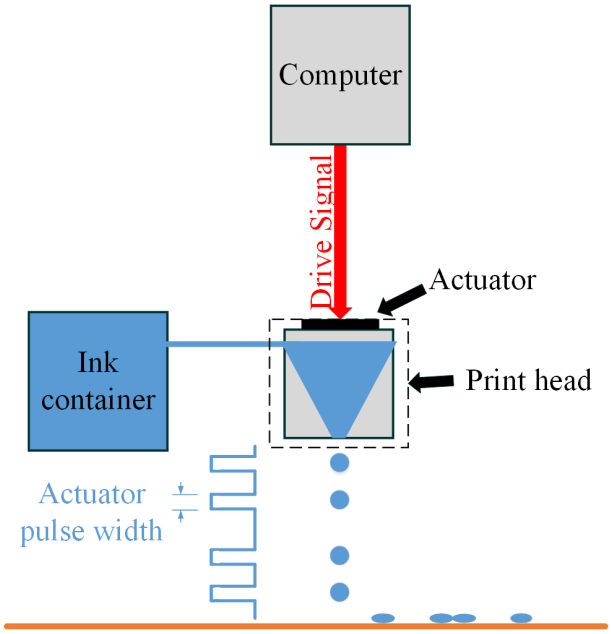

Figure 2.9: Illustration of drop on demand inkjet printing technology.

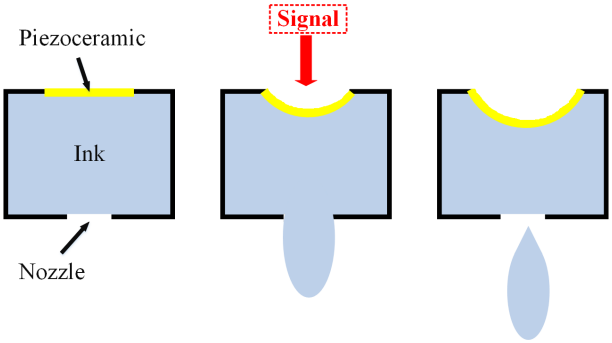

Figure 2.10: Schematic of DOD inkjet printing facilitated with piezoelectric ejection.

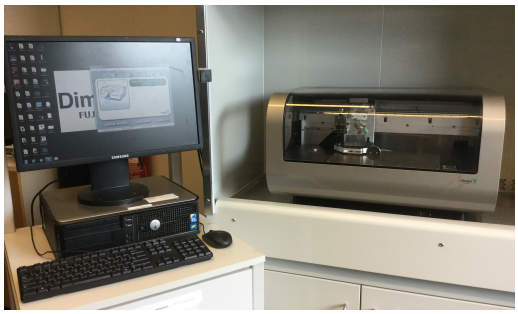

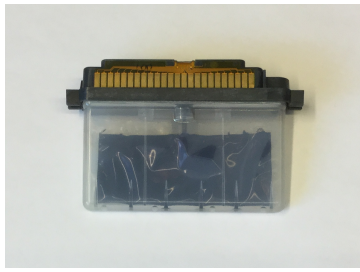

Figure 2.11: (a) Dimatix-2831 inkjet printer, (b) cartridge with a head of 16 nozzles.

of 20-40 centipoise (cps) at the room temperature. High viscosity materials have to be lowered the viscosity to facilitate jetting process. The common solution is to apply heat, adding solvents or other low viscosity materials to the fluid. (Gibson et al. (2015))

The second challenge is to control droplet deposition in patterning process. This includes many significant issues from droplet deposition path to substrate-wetting properties. Furthermore, the droplet size and velocity are effective on the printing process. These parameters must be controlled by nozzle operation and design. The important factors on the results are liquid density, surface tension, print head and design. One of the printing operational challenges are nozzle clogging. In this case, the droplets are prevented from exiting through small nozzles. (Niittynen (2015))

After patterning, the liquid droplets convert into solid geometry. This conversion must be controlled to achieve high quality printed layer or structure. The quality of pattered structure highly depends on the phase change of printed material. The examples are solidification of melted materials, evaporation of solvents, curing of photopolymers, or other chemical reactions. The droplets may solidify non-uniformly resulting undesired outcomes.

The highest print resolution is achieved by producing many small droplets close to each other. This needs many nozzles on print head. However, many manufacturers do not provide high-density nozzle print heads. The other solution is printing multiple layers for the same desired area. (Gibson et al. (2015); Niittynen (2015)) The inkjet printing has wide range of applications such as thin film transistors (TFTs) (Sowade et al. (2016)), magnetic data storage applications (Voit et al. (2003)), sensors (Dankoco et al. (2016); Singh et al. (2010), and biological and pharmaceutical applications (Singh et al. (2010); Zheng et al. (2011)).

2.3.4 Doctor blade

Doctor blade (DB) is a rapid and simple flexographic printing technology. In this method, constant amount of ink can be spread through a mask or stencil and produce a desired pattern on various kind of substrates. The examples of DB technique applications are fabrication of polymer based solar cells (Wengeler et al. (2013)), supercapacitors (Lehtimäki et al. (2014)), and transistors (Xu et al. (2016)).

The DB devices generally work in two different ways either moving substrate with static blade or moving blade across fixed substrate. The first one is used for large area roll-to-roll (R2R) process (Hösel (2013)). In this work, we use DB device with latter technology (see in Figure 2.12).

Nowadays, there are many choices for blade materials and edge profiles due to applications. Steel blades are typically used regarding to high quality and reliable results. The other examples are ceramics typically for abrasive inks, and composite blades for using at high speeds due to their long lifetime.

The effective parameters during fabrication process are the gap between blade and substrate, applicator speed, the surface temperature, and ink condition and viscosity. The thickness of wet layer is determined by the applicator and the thickness of stencil on the substrate. (Berni et al. (2004); Hösel (2013); Wengeler et al. (2013)) The DB manufacturing method is explained in more details in reference (Berni et al. (2004)).

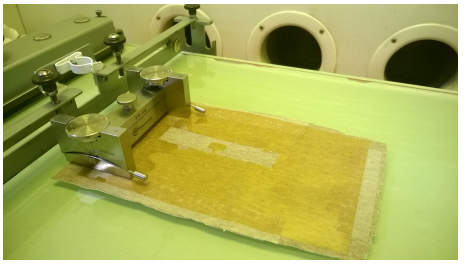

Figure 2.12: Doctor blade device and a substrate covered with mechanical mask. **(Publication V)**

2.4 Post-treatment process after patterning with inks

After ink deposition, it typically requires post-treatment process to achieve and improve final properties for most the end-use applications. The post-treatment is mostly a function of ink and substrate combination rather than printing process. (Gibson et al. (2015); Grunwald et al. (2010))

Depending on ink material, the deposited materials require different post-treatments. Some inks need curing as a post-treatment step. In curing temperature, organic particles start loosing their organic shells. While others need higher temperatures compare to curing temperature to remove organic solvents and force conductive particles close together starting neck formation among particles which is known as sintering. Due to high surface to volume ratio, using of nanoparticles dramatically decreases sintering temperature. (Perelaer et al. (2008))

The most common method for thermal post-treatments are using conventional oven. Most inks need elevated temperatures, which makes them incompatible with low temperature stand substrates such as papers and polymeric substrates. The other alternative techniques are continuous or pulsed laser sintering (Kumpulainen2011570), microwave radiation, and photonic curing by Xenon flash exposure (Sipilä (2016)).

One possibility of post treatment process is subjected the graphene-based printed layer to the pulsed Xenon flashes. In **Publication VIII**, two different curing techniques for graphene-printed samples are studied: oven curing and photonic curing. The photonic curing is carried out by exposure to pulsed Xenon flashes, and it is explained in details in Section 2.4.1. In addition, pulsed Xenon flashes can also be used to reduce graphene oxide particles into RGO with retrieved conductivity. **(Publication II)**

2.4.1 Photonic curing

Photonic curing is a promising alternative to traditional thermal curing processes in printable electronics. In photonic curing process, high intensity pulsed light, originated from a flash lamp, is subjected to the material of functional thin layer on a substrate without damaging it. Additionally, photonic curing reduces the processing time exponentially in the range of milliseconds.

Typically, Xenon is used as the fill gas in flash lamps which provides about 50% quantum efficiency. (Schroder (2011)) The Xenon flash lamps have a broad light spectrum from UV to IR. In general, compressing of energy over a short duration causes higher peak power. As a consequence, peak power phenomenon leads to greater penetration depth

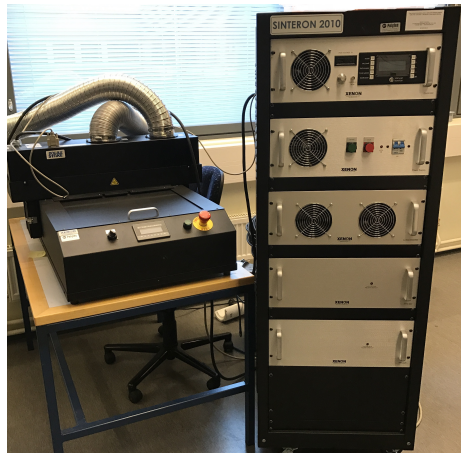

Figure 2.13: Xenon Sinteron 2010-L system.

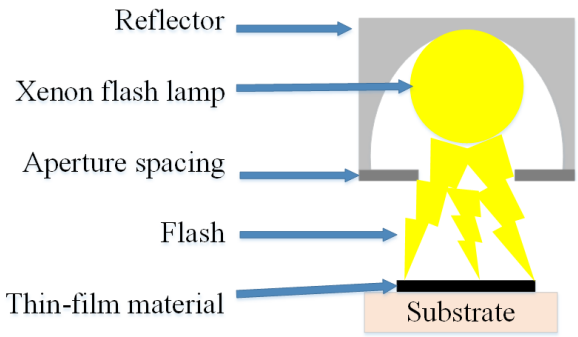

Figure 2.14: Schematic image illustrated a photonic curing system. (Sipilä (2016))

into material. So using of short pulses of light leads to minimal heating which is superior to Mercury based continuous systems. (Panico (2010); Xenon-Corporation (2013))

The braodband emission of Xenon is more flexible than laser. This means some portion of UV to IR emissions can be absorbed by most thin films and lead to cure desired layer. (Schroder (2011))

The photonic curing system consists of Xenon flash lamp, lamp housing, power supply, high voltage capacitors, cooling air system, and controller. The photonic curing machine, which is used in this study, is Xenon Sinteron 2010-L system (Figure 2.13).

The basics of photonic curing system equipped with Xenon flash lamp is presented schematically in Figure 2.14. As it is illustrated in Figure 2.14, the pulsed light from Xenon lamp is originated from lamp and delivered to the thin-film material on the substrate.

The aperture acts as an adjustable light mask to determine the amount of light that reaches to the sample upon each flash. The aperture spacing can be set 10 mm to 80 mm. Moreover, the optimal distance from window to test sample is 25 mm.

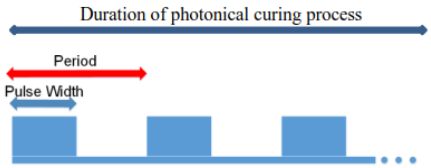

Figure 2.15: The principle of the continuous flash mode. **(PublicationVIII)**

2.4.1.1 Energy calculation

The delivered energy to flash lamp is adjusted by two parameters: high voltage (HV) value and flash time duration. The energy of each pulse (E) is calculated as follows:

$$E = (V/3120)^{2.4} \times t, \tag{2.2}$$

where E, V and t are energy (J), high voltage value (V), and time duration of pulse (μs), respectively. Almost 50 % of the electrical energy is transformed into optical energy. (Xenon-Corporation (2013))

2.4.1.2 Operating modes and parameters in photonic curing

The process parameters completely depend on the operating flash mode. In Sintron 2010, there are four programmable operating flash modes: single, double, continues, and burst mode.

Two basic parameters are common in all four flash modes. First, energy level per unit time, which is known as high voltage (HV) setting. Secondly, time duration of each flash which is determined by pulse width.

In single flash mode, the lamp flashes once, and two basic parameters, (HV) value and pulse width, are adjustable. In double flash mode, the lamp flashes twice, and adjustable parameters are HV value, first and second pulse width, and the time delay from start point of first pulse to second pulse which known as period parameter (see in Figure 2.15). In continuous flash mode, the lamp constantly flashes along with three parameters adjusted as HV value, pulse width, and period parameters, as shown in Figure 2.15. The burst flash mode is similar to continuous mode with additional feature of adjusting number of flashes.

In general, allowable range for HV value is 1800 V to 3100 V, pulse width between 100 μs to 2000 μs, and period value between 100 ms to 5000 ms. (Xenon-Corporation (2013))

2.4.1.3 Advantages of photonic curing

The advantageous of photonic curing are:

- Fast exposure time in milisecond ranges,
- Enable to use temperature sensitive substrates such as paper and wood,
- Capable to cover broad area, and curing selective area,
- Capability to be integrated in high-speed additive manufacturing process such as roll-to-roll or 3D printer devices,

- Enable to built multilayers on top of each other without any concern of thermal stress creation at underlayers,
- Enable to cure copper in air, which normally needs to be cured in reducing or inert medium,
- Clean and cost-effective process.

In photonic curing, thin-film material are heated without heating underlying or adjacent substrate. It is a cost-effective manufacturing method for highly performance microelectronic devices. (Schroder (2011); Xenon-Corporation (2013))

Photonic curing is an alternative to traditional curing methods such as oven and lasers. It can be used in widespread applications from thin-film transistors (TFTs), solar cells to RFID and smart packaging. (Das et al. (2015); Farnsworth et al. (2012))

2.4.2 Post-treatments for graphene oxide

In some cases, the deposited materials need post-treatments consisting of several steps. For instance, the printed graphene oxide ink requires two-step post-treatments: first annealing and then reduction process.

The term annealing generally means as a step toward stress relieving. In inkjet printed thin films, annealing process is also meaning to assist for solvent removal and connected the printed droplets together. This step is as essential process before reduction process. However, annealing is not enough to retrieve the conductivity of graphene oxide layer without subsequent reduction step.

In case of using graphene oxide (GO) based ink, reduction process is essential for removing oxygen containing groups to retrieve conductivity. As explained in Section 2.1, GO changed into reduced graphene oxide (RGO) which has graphene like structure. Basically, the oxygen affects on tuning of band gap. In this process, oxygen concentration is gradually decreased leading to changes in materials' band gap. (Acik and Chabal (2013))

The most common reduction methods are either chemically or thermally reducing of GO. Chemically reduction is carried out at temperatures typically lower than 100 °C by strong chemicals such as hydrazine and strong alkali agents. However, chemical agents have environmentally harsh nature. Furthermore, optimization and repeatability of the chemically reduction results are challenging due to fast kinetics. This causes different achieved properties in each experiment. Another challenge is related to agglomeration of chemical agents in organic solvents, which can be eliminated in case of using chemically and thermally process together. (Acik and Chabal (2013); Yavari et al. (2012))

The thermal reduction of GO is carried out at elevated temperatures. This leads to decrease in oxygen concentration, and consequently formation of defects in RGO. During thermal reduction, trapped water molecules reacts with defects existing in interlayers resulting formation of additional carbonyls. This hinders the subsequent reduction process, which can be partially retrieved by increasing the reducing duration. Reduction ambient has significant effects on oxygen removing process and also lowering working temperature. Different reduction atmospheres can be used such as hydrogen and nitrogen.

The other reduction techniques have been reported such as using microwave for assisting the thermal reduction of GO (Chen et al. (2010)), plasma-assisted techniques, solar electromagnetic radiation (Acik and Chabal (2013))and photothermal heating (Cote et al.

(2009)). One possibility is to use Xenon flash pulses to reduce graphene oxide. The principles of Xenon flash device and its parameters are explained in Section 2.4.1.

3 Materials and methods

This chapter describes different utilized materials including inks and substrates, short description about the printed designs, different additive manufacturing methods, and different post-treatment processes.

In this thesis, three different manufacturing techniques were used: inkjet printing, doctor-blade, and direct writing. The fabrication steps in patterning via inkjet printing are: ink development, surface treatment of substrate, inkjet printing, post-treatments including annealing and subsequently reducing either at reducing atmosphere or pulsed Xenon flashes. **(Publication I and II)**.

The fabrication steps in DB and DW techniques, are illustrated in Figure 3.1. First, graphene ink was deposited on different kinds of substrates. Secondly, the fabricated samples were cured in an oven or subjected to pulsed-flash which is known as photonical curing process. Final step was the attachment of RFID IC. The used tag IC was NXP UCODE G2iL series RFID IC with the wake-up power of -18 dBm (15.8 μW). The IC was mounted by the manufacturer in a fixture patterned from copper on a plastic film. During this step, the $3 \times 3\ mm^2$ pads of the fixture was attached to the deposited antenna pattern with conductive epoxy. The antenna-IC join was cured by leaving it in room condition for 24 hours. (**Publication III-VIII**, Björninen et al. (2014))

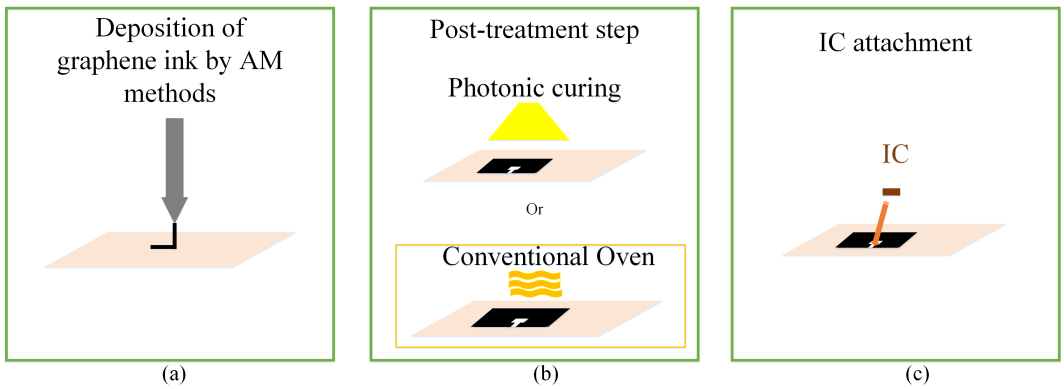

Figure 3.1: Manufacturing of graphene RFID tags: (a) Deposition of graphene ink on the desired substrate. (b) Post-treatment step carried out by either in conventional oven or photonic curing. (c) IC attachment. **(Publication VIII)**

3.1 Materials

3.1.1 Inkjet printable ink

Single Layer graphene oxide (SLGO) was utilized (provided by Cheap Tube Inc.). The average particle size of SLGO is 300-800 nm with thickness of 0.7-1.24 nm. Different concentration of SLGO were dissolved in deionized (DI) water and sonicated with power level of 1000 W. The result is a brown homogeneous GO ink. **(Publication I)**

In addition, graphene oxide/polystyrene (GO/PS) ink was also developed by adding polystyrene solution up to 10 vol.%. The polystyrene solution consists of 1 wt.% polystyrene nanoparticles dispersion in DI-water with a small amount of Tween-20 as a surfactant. **(Publication II)**

3.1.2 Graphene inks suitable for DB and DW

In general, screen printable inks are suitable for patterning via DB and DW devices. In this work, the utilized graphene inks are listed as follows:

1. Functionalized graphene nanoplatelets (GNPs) ink (HDPlas®IGSC02002; Haydale Ltd., UK), which is metal-free, 100% organic (non-tarnishing), environmentally-friendly, and curable at low temperatures. (Hay (2015))

2. Graphene ink (Vor-ink™X103, Vorbeck Materials Corp.), which is high-viscose and electrically conductive ink designed for application by screen printing. (Varma et al. (2012))

3.1.3 Substrate materials

Different kind of substrates were used: kapton, cardboard, stretchable and normal textiles, and wood.

The kapton is a flexible polyimide substrate, and in this work, kapton HN was used with two different thickness of 50 and 125 μm. This polymeric substrate can stand high temperatures up to 400 °C. The kapton substrate needs surface treatment due to hydrophobic nature of kapton and graphene ink. Therefore, wettability of kapton must be enhanced before printing. The surface were treated by two different methods either UV-Ozone (Novascan, PSD-UV series) or Oxygen plasma (Diener Electronic, PICO plasma cleaner).

The normal rough packaging cardboard was used with thickness of 560 μm. The dielectric properties were measured as: relative premittivity of 1.8 and loss tangent of 0.015. **(Publication III)**

Both fabrics were made of 100 % cotton with thickness around 3 mm. The measured relative permittivity and loss tangent were 1.6 and 0.044. **(Publication VI)** The thin wood veneer was used with thickness of 0.65 mm.

3.2 Antenna patterns

Two different antenna patterns were printed in this study. The dipole antenna was fabricated (**Publication III**) and the geometry dimension is shown in Figure 3.2.

The other selected design is shown in Figure 3.3. This was based on a design in reference (Björninen et al. (2014)). This design has input impedance same as of used RFID IC input impedance). (Björninen et al. (2014), **Publication III-VIII**)

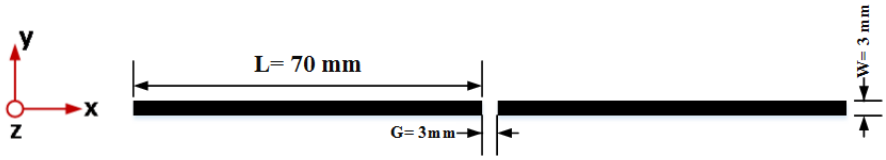

Figure 3.2: Dipole antenna design.

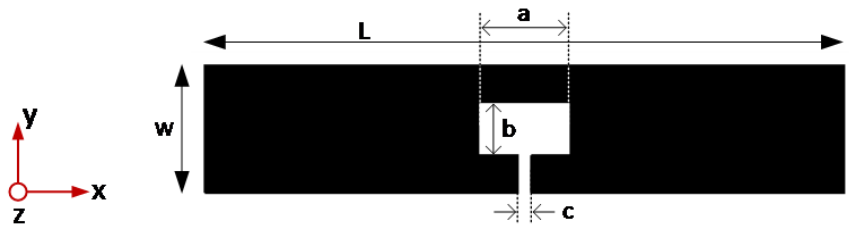

Figure 3.3: RFID tag design.

Table 3.1: Geometrical parameters of RFID tag antenna in millimeters [mm].

L	W	a	b	c
100	20	14.3	8.125	2

3.3 Additive manufacturing methods

The different additive manufacturing methods were used:

3.3.1 3D direct write method

In this study, nScrypt tabletop series micro-dispensing system was used to fabricate the UHF RFID tags on different substrates. In Figure 3.4, the 3D dispenser parts can be seen. The micro-dispenser was equipped with a positive pressure pump which connected to a valve and coupled with a nozzle. The air pressure was applied to the ink-filled syringe, and as a consequence, ink was pushed into the main valve body, and eventually passed through the nozzle tip. The used nozzles were made of ceramic with wide rage of tip diameters regarding ink viscosity, particle size, and the final printing feature size.

This system can be precisely controlled by a computer with an access to a user interface to change and optimize the printing parameters. For instance, the "open and close" value can be customized and controlled along with a constant material pressure. This leads to ability of discrete volumetric control as low as 100 picoliters. This technology makes possible to produce a controllable and consistent material flow rate with the accurate starts and stops. (nSc (2016)) Furthermore, this system is enabled to utilize a wide range of material viscosities.

The other critical parameters can be controlled by computer interface are the adjustment of the distance between the ceramic tip and the substrate and the printing speed. (nSc (2016)) In this study, the used parameters are mentioned in Table 3.2.

In Figure 3.5a, the ready tag is shown which is 3D printed on wood substrate. As it is illustrated in Figure 3.5, the printing direction is along with wood veneer. The printing for this pattern was carried out in 2 parts, and the start and end points for each part are shown in Figure 3.5b.

Table 3.2: Parameters of 3D micro-dispenser.

Inner diameter/outer diameter	125 μm/175 μm
Pressure	16 psi
Printing space	250 μm
Printing angle	0°

3.3.2 Inkjet printing

The developed graphene oxide inks were patterned on treated kapton by FujiFilm Dimatix-2831 inkjet printer. In this work, the printed pattern was rectangular with dimension of 1mm ×4 mm, and 15 layers were printed in each sample. The resolution was adjusted to be 2540 DPI with cartridge temprature of 28 °C.

3.3.3 Doctor-blading (DB) technique

Doctor-blading technique was used to deposit a graphene layer on the desired substrates. The principles of DB process is shown as Figure 3.6. The graphene ink was spread by a blade with constant speed (14 mm/s) through a mechanical mask. The gap width between a blade and the substrate were adjusted at zero level. Thus, the final wet thickness is

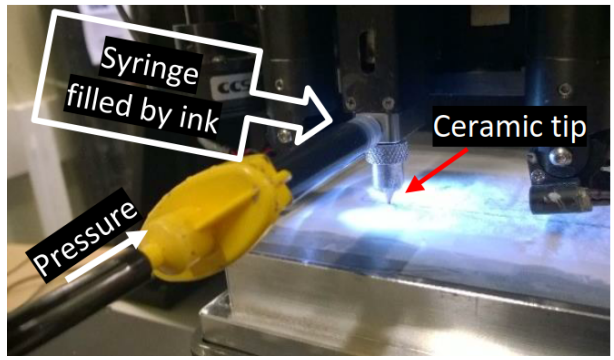

Figure 3.4: 3D micro dispensing system with an ink syringe and a ceramic nozzle tip. **(Publication VIII)**

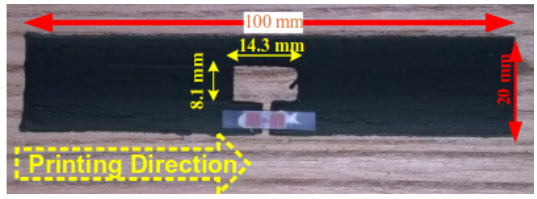

(a)

(b)

Figure 3.5: (a) RFID tag on wood, (b) image of printing direction. **(Publication VIII)**

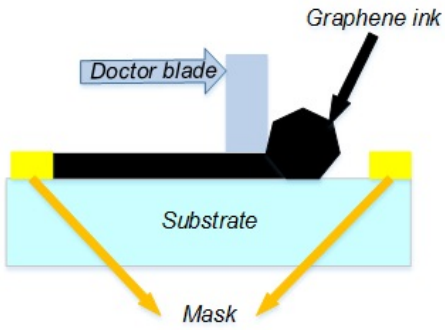

(a)

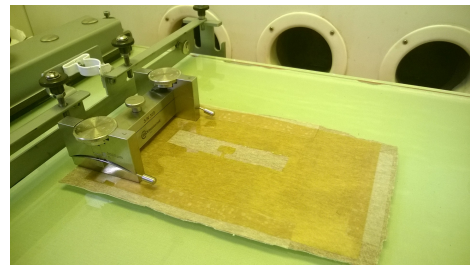

(b)

Figure 3.6: (a) Schematic illustration of doctor-blading method. **(Publication III)**, (b) mechanical mask on a fabric substrate during doctor blading. **(Publication V)**

close to the mechanical mask's thickness. In Figure 3.6b, the mechanical mask can be seen on the fabric substrate. It has the design of RFID tag and made of 50 μm kapton.

3.4 Post-treatments

Based on utilized materials and manufacturing methods, the printed samples need specific post-treatments.

3.4.1 Post-treatments after inkjet printing

In case of inkjet printing of graphene oxide ink, printed GO samples were annealed at 60, 80, and 100℃ for 30 minutes. The optimized annealing temperature was achieved at 100℃ for 30 minutes. After annealing, inkjet-printed graphene-based samples were reduced. In case of using flowing nitrogen gas, samples were heated with the rate of 5 ℃/min up to 200℃, and remained at this temperature for two hours, and finally cooled slowly to room temperature. In case of using argon-15 % hydrogen, the temperature was ramped with the rate of 5 ℃/min, kept at 200℃ for 30 minutes, and then heated up to 300℃ and kept for 30 minutes. In case of using pulsed flash reduction method, the printed samples were subjected to a single flash pulse with adjustable HV and pulse duration. The optimized parameters are discussed in Section 4.1.4.

3.4.2 Post-treatments after DB and DW

The graphene-based samples were fabricated by doctor blade and direct writing, needed just curing to enhance their properties. The samples were cured by either oven or photonically-cured by pulsed Xenon flashes.

The curing in oven was followed as presented in the ink data sheets. (Hay (2015); Varma et al. (2012)) The samples printed by GNP ink were cured at oven at 60℃ for 30 minutes **(Publication V-VIII)**. The Vorbeck graphene printed samples were cured at 130℃ for 4 minutes. **(Publication III-V)**

In photonic curing, the printed graphene patterns were subjected to a series of flashes from a Xenon sintering system (Sinteron 2010-L, Xenon Corp.), where the distance from the test sample to the window of the lamp housing was 25 mm.

In this work, the operating mode was set on continuous mode, since a single pulse was not enough to cure the graphene layer and left it wet. As explained in Section 2.4.1, three parameters are adjustable in the continuous mode: high voltage (HV) value, pulse width, and period. In order to optimize the continuous mode parameters for graphene layers, a static pulse width and period were used, while the voltage value and the number of pulses were manipulated. The achieved optimized parameters are varied depending the thickness and materials of substrate. **(PublicationVIII)**

In general, the samples are subjected to the pulses with the lowest energy and gradually increase the energy level to find the optimum photonic curing parameters. This is followed by gradual increase in conductivity of samples and undesired mechanical detachment from substrate. By optimizing curing parameters, the printed samples gained highest possible conductivity along with maintaining the mechanical durability.

4 Results and discussion

4.1 Inkjet printing of graphene-based ink on a flexible substrate

Graphene has hydrophobic nature leading to poor solubility in the polar solvents and forming unstable inks. Therefore, graphene oxide is typically used as an alternative material which has hydrophilic nature, and as it is reported in (Le et al. (2011)) soluble in water up to 1 wt.% concentration.

In this study, the graphene oxide (GO) ink and inkjet printing process was optimized. The GO ink was printed on the flexible kapton substrates. The sheet resistance, conductivity, and microstructure of patterned GO was characterized in **Publication I**. The jettable ink must meet viscosity requirement. The ideal viscosity is at the range of 10 cps to 12 cps. The optimized concentration of GO was found to be 0.4 wt.% in DI-water. The viscosity of ink was measured at 28 °C which was around 3.5 cps. Although the viscosity of ink is low, it can be jetted by manipulating the voltage of piezoelectric nozzles as a function of time forming desired spherical droplets. The used jetting waveform and formed droplets are shown in Figure 4.1.

The sheet resistance (R_t) is generally a reliable factor for 2D materials and can be calculated as follows:

$$R_t = \frac{\rho}{t}, \tag{4.1}$$

where ρ and t represent resistivity and film thickness, respectively. In this work, resistance (R) is obtained by applying constant current (I) and measuring voltage (V) based on:

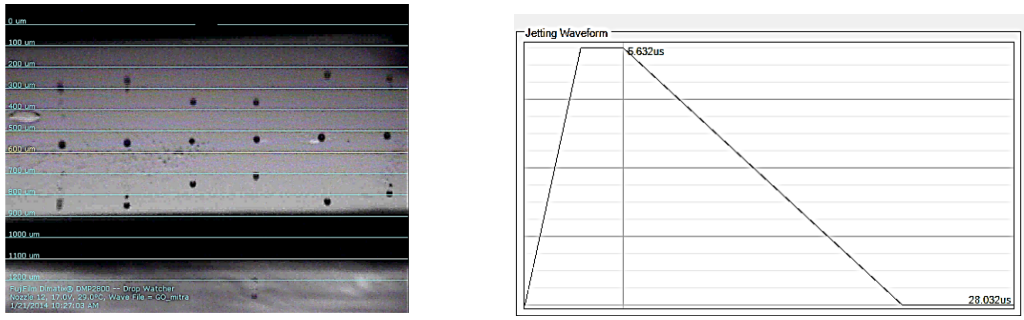

(a) **(b)**

Figure 4.1: (a) Formation of spherical droplets with assisting of (b) jetting waveform. **(Publication I)**

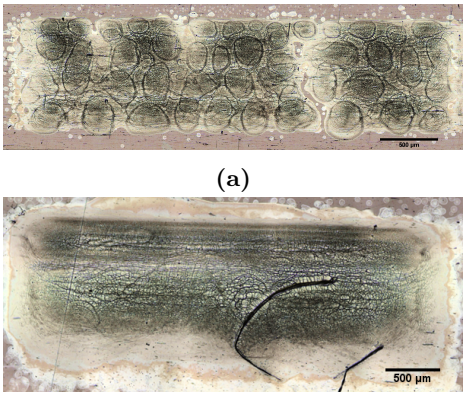

(a)

(b)

Figure 4.2: Laser microscopy images of graphene inkjet printed on treated kapton by (a) UV-Ozone and (b) Oxygen plasma. **(Publication I)**

$$R = \frac{V}{I}, \tag{4.2}$$

By replacing measured R in the following formula, $(\frac{\rho}{t})$ can be achieved, which is known as sheet resistance based on Equation 4.1:

$$R = \frac{\rho}{t}.\frac{L}{W}, \tag{4.3}$$

where L and W represent length and width of printed film, respectively. The conductivity of printed layer is obtained as below:

$$\sigma = \frac{1}{\rho}, \tag{4.4}$$

4.1.1 Surface treatment effect

The optimized GO ink has poor wettability on untreated kapton showing contact angle of 64.2 °. As a result, the kapton substrate was subjected to two different surface treatments either oxygen plasma or UV-Ozone to modify wettability property. The measured contact angles were 56.8 ° and 26.1 ° after UV-Ozone and oxygen plasma treatment, respectively. In Figure 4.2, two identical samples were shown which prepared with two different surface treatment. The Oxygen-plasma treated sample is shown lower sheet resistance of 2124 (Ω/sq) and higher retrieved conductivity (160 S/m) due to better spreading and overlapping of printed droplets. While, the printed droplets still has kept their shape on UV-Ozone treated sample, showing unconnected droplets leading to low conductivity (56.64 S/m).

4.1.2 Annealing effect

Before reduction process, samples must be annealed. Otherwise, the printed samples remain non-conductive even after reduction. Annealing is a necessary step resulting

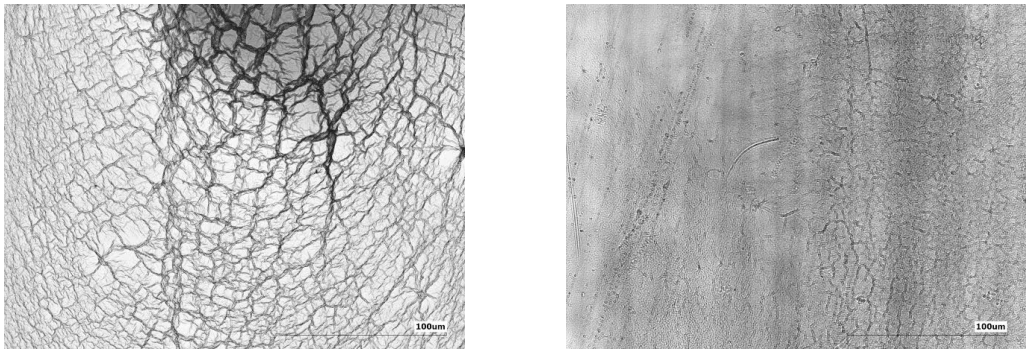

(a) **(b)**

Figure 4.3: The microstructure of RGO layer at flowing nitrogen with two different GO ink concentration: (a) 0.4 wt.% and (b) 0.2 wt.%. **(Publication I)**

connected printed droplets. The optimized annealing condition was found to be at 100 °C for 30 minutes in **Publication I**.

4.1.3 Ink concentration effect

The concentration of graphene oxide in ink also plays an important role on the final achieved sheet resistance. Higher amount of graphene oxide particles can be reduced during thermal reduction improving conductivity. According to achieved results, the reduced GO samples printed with concentration of 0.4 wt.% GO and thermally reduced at nitrogen atmosphere shows conductivity of 22.86 S/m, and covered with more wrinkles and cracks (Figure 4.3a). While similar sample printed with 0.2 wt.% GO has conductivity of 8.25 S/m, and covered with less wrinkles (Figure 4.3b). The cracks and wrinkles indicate that higher amount of RGO has been formed.

4.1.4 Thermal reduction effect

In thermal reduction, the effective factors are reducing atmosphere, temperature, and aging time. In **Publication I**, the different effects of reducing atmospheres are studied. The printed GO samples obtain metallic luster appearance regardless of atmosphere. This originates from improving carrier concentration and mobility, and as a consequence, boosting the reflection of incident light.

The reduced samples at Ar-15%H_2 have conductivity about 160 S/m. While, nitrogen reduced sample has conductivity of 22.86 S/m. This can be as a result of reducing agent size. The nitrogen is not as small as hydrogen to penetrate into deep layers. This causes lower amount of reduced graphene oxide. As a result, the conductivity obtained at Ar-15%H_2 atmosphere is considerably high.

4.1.5 Photonical reduction effect

The pulsed Xenon flashes can be used as an alternative reduction method with no need for high temperature which is investigated in **Publication II**. The photonic reduction is tunable by the amount of exposure energy. The challenge of photonic reduction is uncontrollable dimensional changes. By exposing to longer pulses with higher voltage

(a) **(b)**

Figure 4.4: Microstructure of RGO/PS printed samples (a) without annealing, (b) with annealing. **(Publication II)**

value, the formed RGO was fully detached from substrate. This originates from fast degassing of printed graphene oxide resulting exceptional expansion of graphene oxide. (Cote et al. (2009))

In **Publication II**, the suggested solution is adding polystyrene nanoparticles dispersion in DI-water to the prepared graphene oxide ink, named as graphene oxide/polystyrene (GO/PS) ink. The benefits of using polystyrene nanoparticles is easily dissolving in graphene oxide ink along with relative low temperature. The GO/PS ink is jettable and can be inkjet printed with similar voltage waveform in Figure 4.1b, by increasing firing voltage from 20 V to 25 V. The droplets of GO/PS ink has contact angle of approximately 50 ° on untreated kapton. This shows GO/PS ink is hydrophobic and it needs surface treatment of kapton substrates. The treated kapton with oxygen plasma shows the contact angle of about 20 ° for GO/PS ink.

The printed GO/PS layer on kapton samples were subjected to a single pulsed Xenon flash with different hight-voltage value and duration. The optimized reduction has been done under a single pulse with high voltage value of 1800 V for 1400 μs. The calculated energy of each pulse is 374 J (by Equation 2.2) with the transfered optical energy of 2.43 J/cm^2.

Additionally, it is shown in **Publication II** that annealing before flash reduction assists removing of water. This lowers the probability of instantaneous decomposition of graphene oxide which happens during flash reduction and consequently improves the adhesion of printed layer (see in Figure 4.4). The R_t of RGO/PS printed layer on treated kapton is about 1000 Ω/sq which shows Xenon flash improves the reduction process compared to sheet resistance of thermally reduced GO at Ar-15%H_2 atmosphere, which was reported 2124 Ω/sq in **Publication I**.

The result RGO/PS has porous and fluffy structure. The durability of RGO/PS is enhanced as a result of heat sink effect of polystyrene nanoparticles. (Cote et al. (2009)) This means PS nanoparticles are melted to fuse with reduced graphene oxide particles. Additionally, the adhesion of printed RGO layer is enhanced by using polystyrene nanoparticles. The interface of reduced graphene oxide and polystyrene composite with kapton substrate is shown in Figure 4.5.

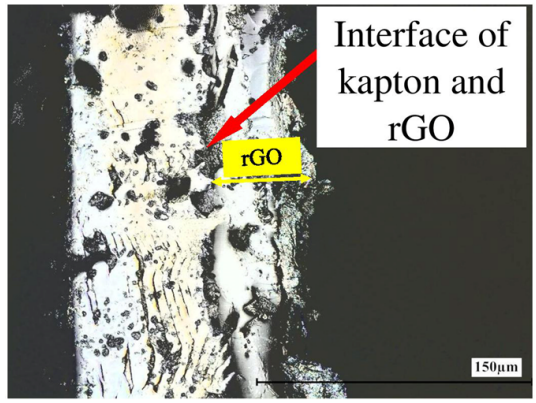

Figure 4.5: Cross-section of RGO/PS composite on kapton. **(Publication II)**

4.2 Using doctor blade technique to fabricate graphene-based RFID tags

The graphene screen printable ink was patterned on desired substrates via doctor blading technique. In **Publication III**, it is completely explained the fabrication method and discussed about two patterned samples: dipole antenna and RFID tag as it is shown in Figure 4.6.

The sheet resistance (R_t), thickness (t), conductivity(σ), and resistivity (ρ) of printed sample were measured and shown in Table 4.1. The thickness of printed graphene patterns were measured by Alicona optical profilometer. According to Figure 4.7a, the thickness varies in the range of 30 to 60 μm. However, some peaks can be seen as a result of ink agglomeration on the surface. The average thickness of RFID tag and dipole antenna are 42 and 38 μm, respectively. The cardboard has rough and porous structure leading to ink penetration up to 30 μm (see in Figure 4.7b).

The S11 value, radiation pattern, realized gain are measured in dipole antenna. According to Figure 4.8a, measured $S11$ shows minimum values of -15.5 dB at frequency of 876 MHz. The antenna shows a broadband behavior. Figure 4.8b shows the dipole antenna has a

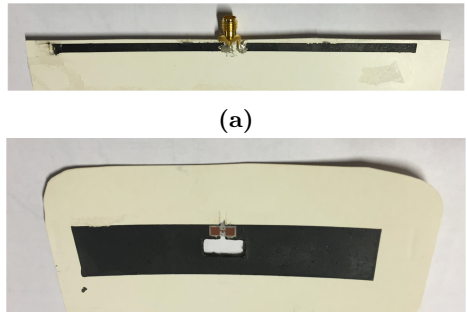

(a)

(b)

Figure 4.6: Graphene based: (a) dipole antenna on cardboard, and (b) RFID tag on cardboard. **(Publication III)**

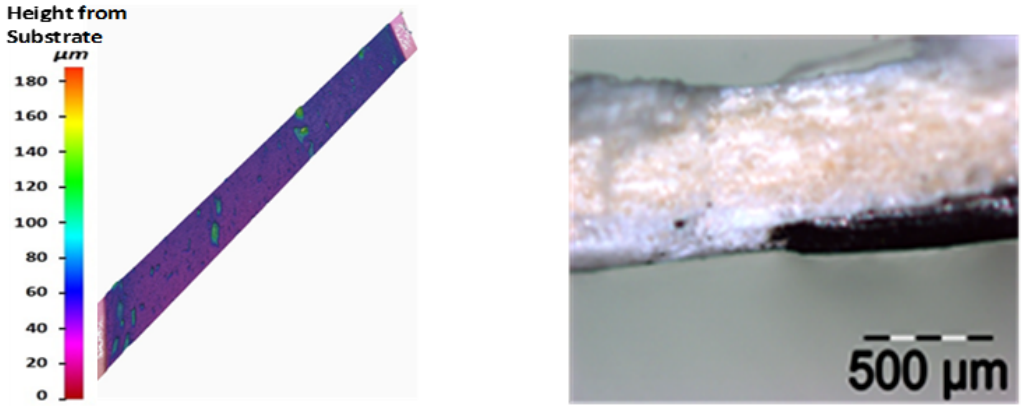

(a) **(b)**

Figure 4.7: (a) 3D profile of graphene patterned on cardboard, and (b) the cross-section of patterned graphene on cardboard. **(Publication III)**

Table 4.1: The measured properties of patterned samples. **(Publication III)**

Antenna pattern	R_t [Ω/sq]	ρ [Ω.m]	[S/m]	t [μm]
Dipole	1.9 ± 0.1	7.9×10^{-5}	1.25×10^{4}	42
RFID tag	1.9 ± 0.1	7.2×10^{-5}	1.39×10^{4}	38

maximum 40% total efficiency and -2.18 dBi realized gain at 889 MHz. The low value of efficiency is as a result of low radiation efficiency and low conductivity of graphene laminate. According to Figure 4.8c, H-plane and E-plane radiation patterns are close to ideal dipole antenna radiation patterns. The radiation patterns of this dipole antenna was measured at 875 MHz based on $S11$ plot.

Figure 4.9a illustrated the simulated and theoretical read range values of the RFID tag. The simulation was carried out based on the achieved sheet resistance and thickness values (mentioned in Table 4.1) by ANSYS HFSS ver. 15. Figure 4.9b shows E-plane and H-plane realized gain radiation pattern at 950 MHz. The more details about the realized gain are explained in **Publication III**. The theoretical read range was simulated based on reference (Fu et al. (2015)) and achieved to be over 5 meters and realized gain is -7 dBi. This RFID tag has been originally designed for 940 MHz. (Björninen et al. (2014))

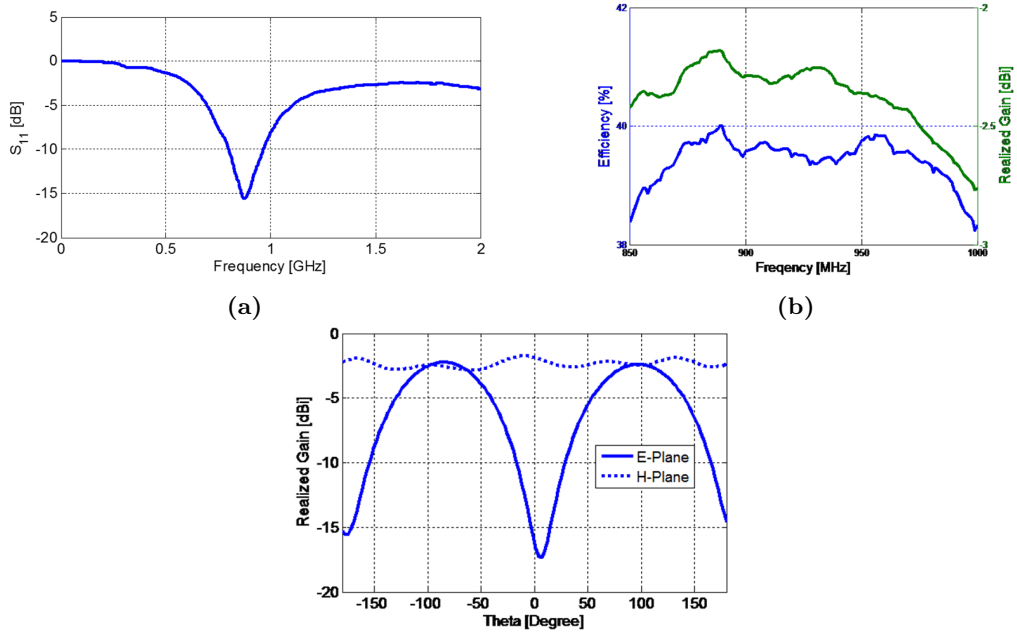

Figure 4.8: Measured parameters for dipole antenna: (a) $S11$, (b) efficiency, and (c) E-plane and H-plane realized gain radiation pattern at 876 MHz. **(Publication III)**

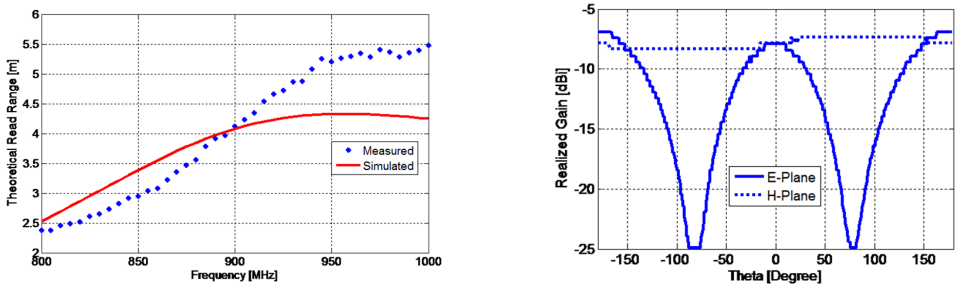

Figure 4.9: Measured parameters for RFID tag antenna: (a) measured and simulated read range value, and (b) E-plane and H-plane realized gain radiation pattern at 950 MHz. **(Publication III)**

4.2.1 Graphene-based vs metallic passive UHF RFID tags

The performance of passive graphene-based RFID tags are compared with silver and copper RFID tags in **Publication IV**. In this study, brush-painting was used as a simple method to fabricate the metallic RFID tags on the cardboard by means of a brush and a stencil. This method is a one-step process and explained with more details in reference (Sipilä et al. (2014)).

Here, the metallic ink is dispensed directly from the brush to the antenna area on the

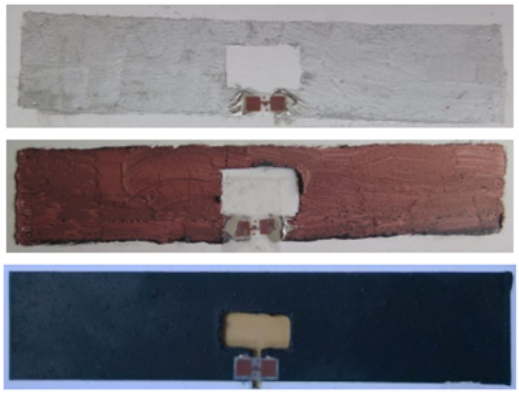

Figure 4.10: The fabricated RFID tags on cardboard made of: silver (top), copper (middle), and graphene (bottom). (**Publication IV**)

cardboard through a 50 μm thick polyimide stencil. The used metallic inks were Metalon-021LV water-based silver flake ink and Metalon-ICI-021 water-based copper oxide ink. After brush-painting of tags, they were sintered by Xenon Sintron 2010-L flash lamp photonic sintering system. The copper oxide ink typically needs the photonic sintering since conventional heat sintering process causes forming of undesired insulated oxide layer. (Kim et al. (2009); Sipilä et al. (2014)) The optimized sintering parameters were studied in reference (Sipilä (2016)). The copper tags were exposed to a single flash pulse with a voltage value of 2200 V with pulse duration of 2000 µs. The silver tags were subjected to two flash pulses with a voltage value of 2000 V and pulse duration of 2000 µs. The used graphene tag was manufactured by DB technique using graphene ink (Vor-inkTM X103) and dried in a conventional oven for 4 minutes at 130 °C.

The fabricated tags and the microscopic images are shown in Figure 4.10 and Figure 4.11. According to Figure 4.11, the copper and graphene tags have small cracks and nonuniform morphology, while the silver tag has the smoothest surface. Furthermore, the average thickness of fabricated tags were measured by highly flexible optical 3D measurement system (Alicona optical profilometer) and the measured average thicknesses are shown in Table 4.2.

The tag performance is evaluated through wireless tag measurements under the European RFID transmission regulations which is explained in Section 2.2.2. The read range values of silver, copper, and graphene RFID tags on cardboard substrate are shown in Figure 4.12 and Table 4.2. The highest attainable read range belongs to silver tags which is aver 12 m, and the read range throughout the global UHF RFID band is over 6 m. The graphene and copper tags shows shorter attainable read ranges of 5.5 and 8.5 m, respectively and the read range throughout the global UHF RFID band is over 5 and 2 meters for the copper and graphene tags, respectively.

According to wireless performances, the graphene tags are promising candidates in antenna fabrication in terms of cost-effective and eco-friendly aspects. The material costs drastically decreases by using graphene-based materials instead of traditional metallic components in wireless applications.

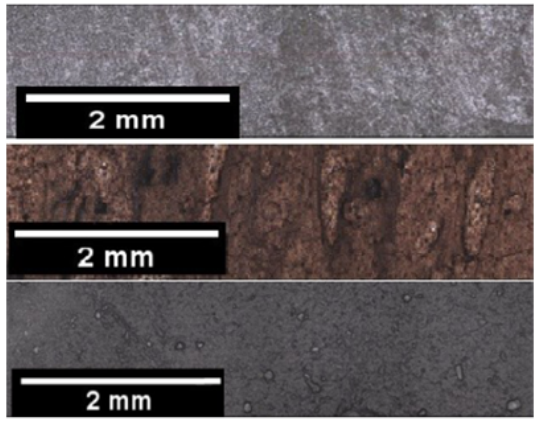

Figure 4.11: Microscopic images (with a magnification of 10X) of fabricated RFID tags on cardboard made of: silver (top), copper (middle), and graphene (bottom). (**Publication IV**)

Table 4.2: The measured properties of tags including cost of each ink. **(Publication IV)**

Material of tag	Average thickness [μm]	Read range peak value [m]	Price
Silver tag	10	12	1000 \$/500g
Copper tag	39	8.5	400 \$/500g
Graphene tag	40	5.5	250 \$/500g

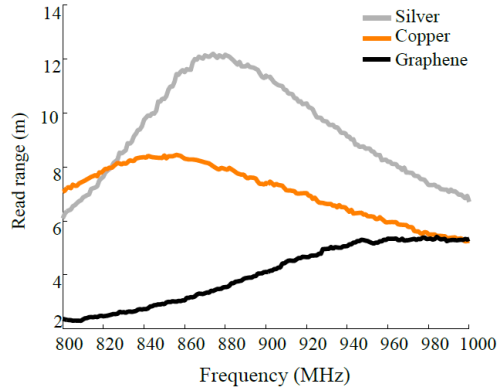

Figure 4.12: Read range values of passive copper, silver, and graphene UHF RFID tags on cardboard. (**Publication IV**)

4.2.2 Graphene-based tags on fabric substrates by doctor blade technique

The fabrication and performance of textile graphene-based passive UHF RFID tags are investigated in **Publication V**. In this part, the main focus is to fabricate graphene tags on stretchable cotton-based fabric substrate.

Doctor-blading technique is used as the fabrication method with two different graphene inks, HDPlas®IGSC02002 and Vor-ink™X103, to manufacture two tag antennas, named

Table 4.3: The specifications and measured properties of textile passive graphene-based RFID tags. (**Publication V**)

Tag	Graphene ink	Substrate	R_t $[\Omega/sq]$	Read range peak $[m]$
TF1	HDPlas®IGSC02002	Stretchable cotton	12.4	1.6
TF2	Vor-ink™X103	Stretchable cotton	3.4	2.4

as TF1 and TF2, respectively. The ready tags can be seen in Figure 4.13.

As shown in Table 4.3, the 4-point sheet resistance of TF1 and TF2 materials were 12.4 Ω/sq and 3.4 Ω/sq, respectively. The precise thickness of printed graphene layer cannot been measured due to harsh curvature of the samples. Figure 4.14a shows a 3D cross-section image of TF2, indicating decrease in thickness of fabric layer (∼2.5 mm) as a result of ink absorption into textile structure.

Figure 4.14b shows the read range values of both graphene-based RFID tags on fabric. The TF2 tag has a higher attainable read range (approximately 2.4 m), while the TF1 tag has a shorter attainable read range (about 1.6 m). In addition, the read range throughout the global UHF RFID band is over 2 m for TF2, and between 1.25-1.5 m for TF1. The difference in the attainable read ranges is explained by using different binders and ingredients in both inks, resulting different sheet resistances, and consequently different wireless performance.

Figure 4.13: The graphene RFID tag fabricated by DB technique on fabric: TF1 (upper) and TF2 (bottom). **Publication V**.

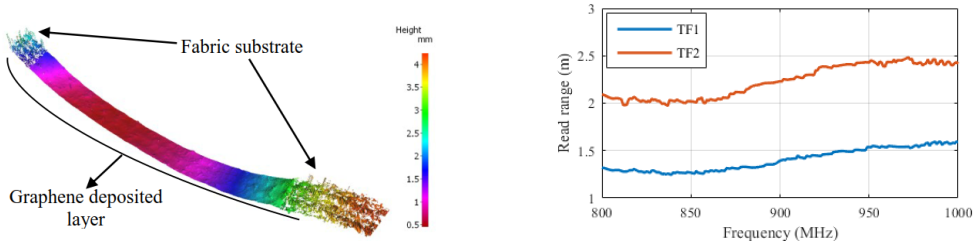

(a) **(b)**

Figure 4.14: (a) A 3D image of a cross-section of graphene RFID tag fabricated by DB technique, and (b) read range values of fabric RFID tag over UHF band. **(Publication V)**

4.2.3 Environmental sensing and reliability study

In this study, GNP ink (HDPlas®IGSC02002) was doctor-bladed on a cotton fabric substrate as explained in Section 3.3.3 (see the ready tag in Figure 4.15). The 4-point sheet resistance (R_t) of graphene tag was measured to be 12.4 Ω/sq.

The graphene ink absorbed approximately 1 mm into the textile. According to microscopic image in Figure 4.16, the structure of deposited area is similar to the fibers pattern, indicating graphene absorbed into the fibers.

The tag performances were evaluated in different conditions: high humidity, bending, or stretching. In the bending test, the tags were bent over a structure with thickness of 30 mm in Y direction, as shown in Figure 4.17a. The wireless performance of tags were measured before and during bending. Additionally, the tags performance were evaluated after 10, 25, 50, and 100 bending cycles at non-bended state. In stretching test, the read range of tag was measured at before/under/after stretching up to 10% of its

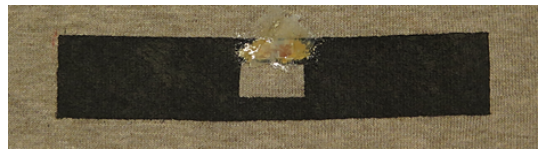

Figure 4.15: Graphene RFID tag on cotton fabric. **(Publication VI)**

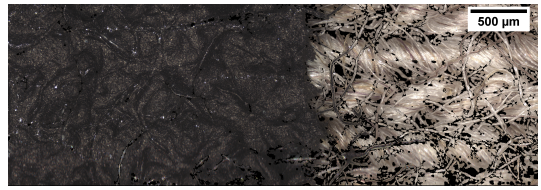

Figure 4.16: Antenna microstructure showing fibers and deposited graphene boundary. **(Publication VI)**

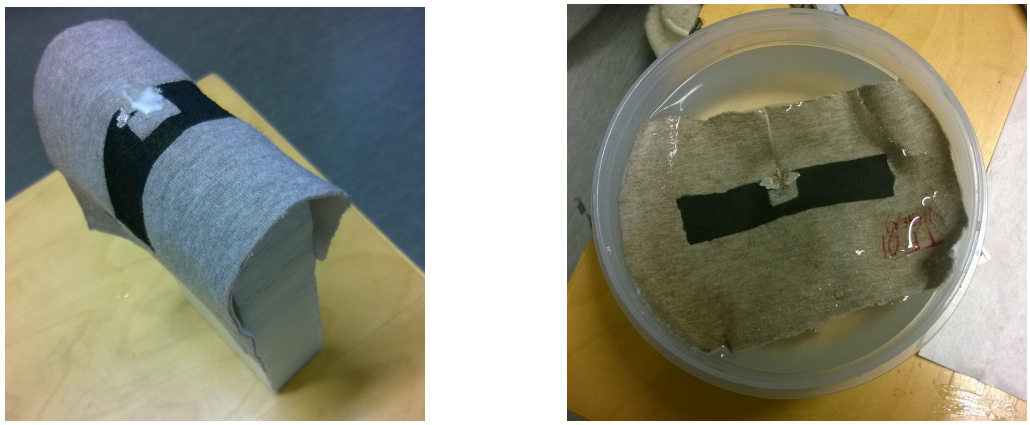

(a) **(b)**

Figure 4.17: Graphene RFID tag at (a) bending test, and (b) hight humidity condition. **(Publication VI)**

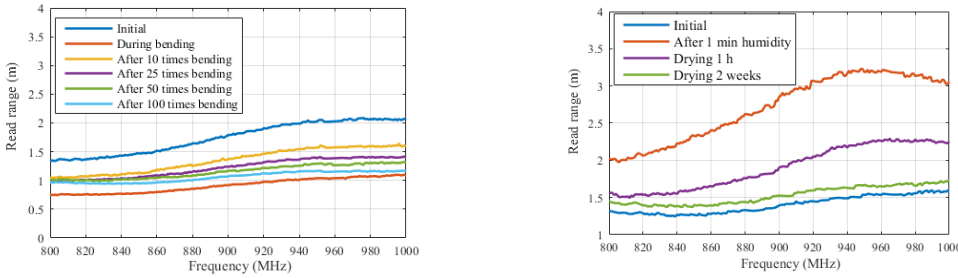

Figure 4.18: Read range of graphene tags related to (a) bending test, and (b) 100% RH condition. **(Publication VI)**

initial length. In humidity test, the tags performance were tracked before and after high humidity test. The tags were placed in a container, filled with tap water (pH=6.5-7), as shown in Figure 4.17b. The wireless tag measurements were carried out before the test, and instantly after one minute in water container. Then, the tags were dried in room conditions and were again measured after one hour and two weeks.

The result of wireless performances at different tests are illustrated in Figure 4.18. According to tag's response, the peak read range of tag is initially about 1.6 m to 2 m at the frequencies of 980-100 MHz. This results are appropriate for many wireless applications.

As shown in Figure 4.18a, the tag's read range was below 1 m under bending test. After more bending cycles, the read range, which measured at a non-bended state, was also gradually decreased, and finally the peak read range measured to be about 1.1 m after 100 bending cycles. This shows the tag can stand harsh bending situation.

The tag read range raises to 3.2 m at the frequency range of 950-965 MHz, when it is measured after exposing to water for 1 minute. The measured read rang shows it gradually reduced back to normal after drying. Due to humidity in office condition, drying cannot be completed to initial stage similar to dried tag in oven. Therefore, the read range even after 2 weeks is slightly different from initial measurement.

The read range of graphene tag increased over 3 m in presence of humidity. This most probably originates form the fact that resistance decreases by increasing humidity level in graphene as shown in other references (Schedin et al. (2007); Smith et al. (2015)). The water molecules affect on resistivity in graphene devices as a result of band gap opening and the key impact of water playing as an acceptor (Schedin et al. (2007); Zakaryan and Aroutionian (2015)). The DC resistance was measured from corner to corner of antenna: about 10 kΩ at room condition, and 2 kΩ after one minute in water. The relative decrement of resistance in presence of humidity is correlated with increase in the read range values. It should be considered that moisture can affect tag's impedance matching and dielectric properties of substrate (Stoppa and Chiolerio (2014)), which typically have effects on reducing read range and shift in peak frequency. Here, the effect of humidity on graphene is stronger that the impact of humidity on textile.

After first stretching cycle, the tag did not respond. This is as a result of micro cracks forming orthogonal to the dipole axis, causing substantial discontinuous (see in Figure 4.19).

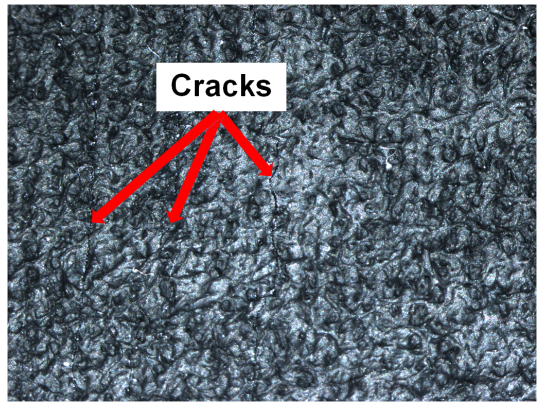

Figure 4.19: Microstructure of Graphene RFID tag on cotton fabric, containing major cracks occurred after stretching. **(Publication VI)**

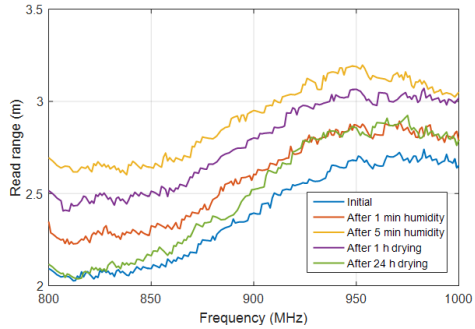

Figure 4.20: Read range values of graphene RFID tag on cardboard related to humidity test. **(Publication VII)**

The humidity test was also carried out with doctor-bladed graphene tag on cardboard, which utilized the "HDPlas®IGSC02002" graphene ink **(Publication VII)**. The measured sheet resistance was 7.1 Ω/sq and the average thickness of graphene layer on cardboard was measured to be 36.4 μm. The tag performance was measured at different stages: before humidity test, instantly after immersing in water for 1 minute and 5 minutes, and after drying at room condition for 1 hour, 24 hour, and two weeks (see in Figure 4.20). First, the tag showed peak read range of 2.7 m at 965-990 MHz frequencies. The read range increased to the 3.2 m at 950 MHz after 5 minutes in water. This results are in line with the effect of humidity on fabric-based tags and the unique response of graphene tags to humidity.

4.3 3D direct-writing and photonic-curing of graphene-based passive RFID tags

In **Publication VIII**, the main focus is to manufacture graphene passive RFID tags by 3D micro-dispenser and subsequently cured either at conventional oven or photonically by pulsed Xenon flashes. The main focus is integrating 3D wiring and photonic curing together with using different green materials as a substrate.

The photonic curing was carried out via Xenon sintering system which enables to utilize different flash modes. The optimum curing was achieved as dispensed samples exposed to contentious mode, which is several pulses with desired high-voltage (HV) value and duration, with adjustable interval timing between each pulses. The curing parameters were optimized by measuring the resistance of cured samples with printed 10 mm graphene line on cardboard. The printed lines were exposed to pulses with HV value in the range of 1900 V- 2300 V. While, fixed amount of pulse width (2100 μs) and period (1100 ms) were utilized. The pulses above 2300 V cause cardboards to burn. According to Table 4.4, the resistance of printed line was measured to be about 35 Ω by using eight pulses with HV of 2200 V. This is close to the resistance of oven-cured sample. The highest resistance belongs to non-cured sample, which was dried at room condition, indicating curing step is an essential and required process to retrieve conductivity.

The HV value must be lowered to about 1900 V, if the wood or fabric substrate are used as they show flammability to stronger pulses. The optimized photonic curing parameters for graphene printed patterns are mentioned in Table 4.5.

Table 4.4: Resistance of a printed graphene line on cardboard with different curing parameters. **(Publication VIII)**

Curing method	Room	Oven	Photonic curing (HV [V], number of pulses, duration of whole curing process [s])							
Parameters	24 h	60 °C 30 min	1900V 8 15 s	1900V 16 30 s	2100V 8 15 s	2100V 24 45 s	2200V 8 15 s	2200V 16 30 s	2300V 8 15 s	2300V 16 30 s
R [Ω]	60	29	40	32	40	27	35	32	35	45

Table 4.5: Optimized photonic curing parameters for different substrate materials. **(Publication VIII)**

Substrate	High voltage [V]	Pulse width [μs]	Number of pulses	Period [ms]	Duration of whole curing process [s]
Cardboard	2100	2100	8	1100	15
Wood	1900	2100	6	1100	11
Fabric	1900	2100	6	1100	11

Table 4.6: The read range values, thickness, average thickness gradient, and sheet resistance of each tag. **(Publication VIII)**

	Substrate	Curing method	Read range [m]	Thickness [μm]	Thickness gradient [μm]	4-point sheet resistance [Ω/sq]
C1	Cardboard	Oven	4.8	17.6	35	31.84
C2	Cardboard	Photonic	5.4	74	140	31.25
W1	Wood	Oven	3.6	91.2	90	27.40
W2	Wood	Photonic	4	67	100	26.08
F1	Fabric	Oven	4.5	29.6	30	68.49
F2	Fabric	Photonic	4.6	51.3	80	48.50

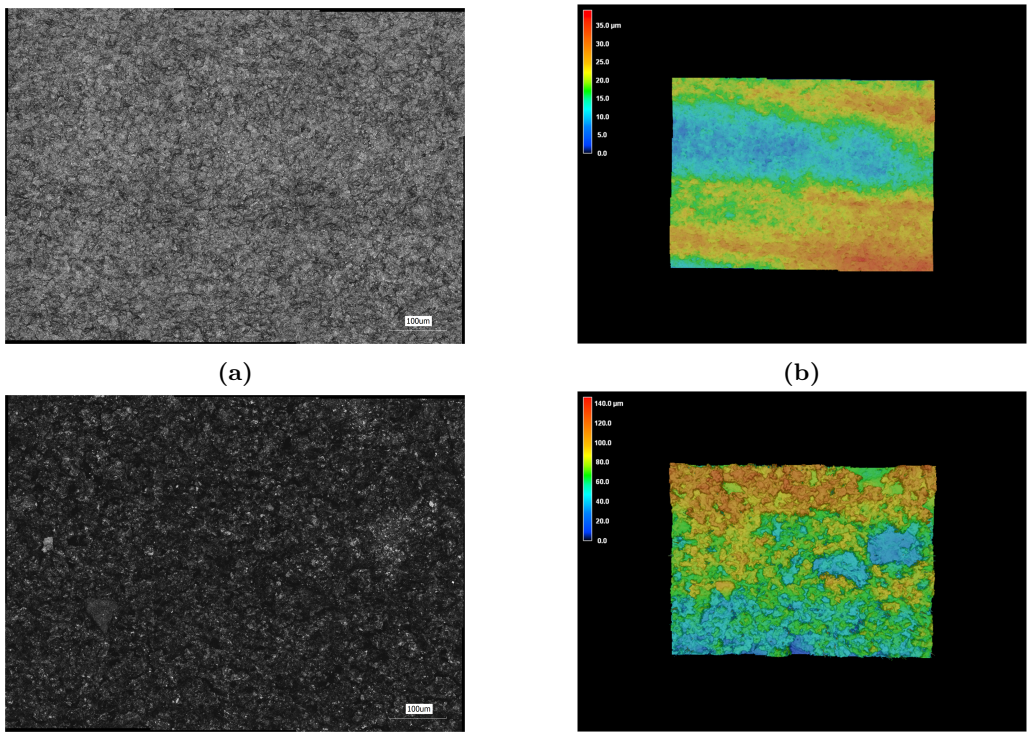

Figure 4.21: (a, c) Laser microscopic images of C1 and C2, (b, d) 3D topography of C1 and C2. **(Publication VIII)**

As it is explained in Section 3.3.1, the graphene passive tags were directly dispensed by 3D micro-dispenser on different substrates: wood, fabric and cardboard; and cured either by oven or Xenon flash pulses. The samples specification and properties can be observed in Table 4.6.

A 3D laser microscope was used to characterize the printed surface microstructure and 3D morphology of sample C1 and C2, as shown in Figures 4.21. The 3D morphology images of other samples can be seen in **Publication VIII**. According to the result presented in Figures 4.21 and Table 4.6, the oven-cured graphene surface (C1) has uniform structure with small difference between highest and lowest points. While photonic-cured sample (C2) has less uniform surface with larger thickness gradient. In addition, oven-cured samples shows higher R_t compared with photonic-cured.

Figure 4.22 presents SEM cross-section image of sample C2 (photonically cured antenna on cardboard). According to image of interface between the graphene layer and the substrate, graphene ink has penetrated into cardboard to about a 20 μm thickness.

Figure 4.23 presents the read ranges of the 3D printed graphene RFID tags on cardboard, wood, and textile, subsequently cured by either oven or Xenon flashes. Based on the results presented in Figure 4.23 and Table 4.6, all photonic-cured tags cover longer read ranges compared to similar oven-cured samples. For example, the highest read range value for a photonic-cured tag on cardboard (C2) is measured to be about 5.4 m, while oven-cured tag (C1) shows read range peak about 4.8 m.

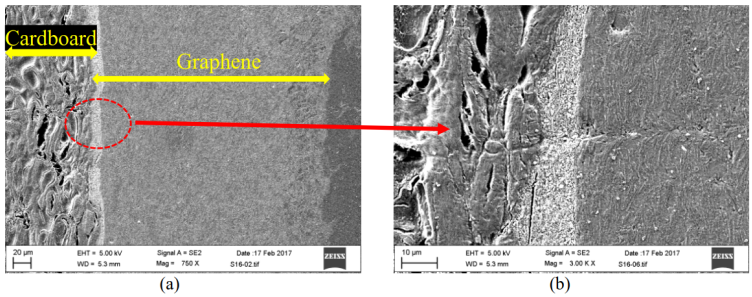

Figure 4.22: SEM images of cross-section area of C2, indicating the interface of grahene penetrated into cardboard substrate. **(Publication VIII)**

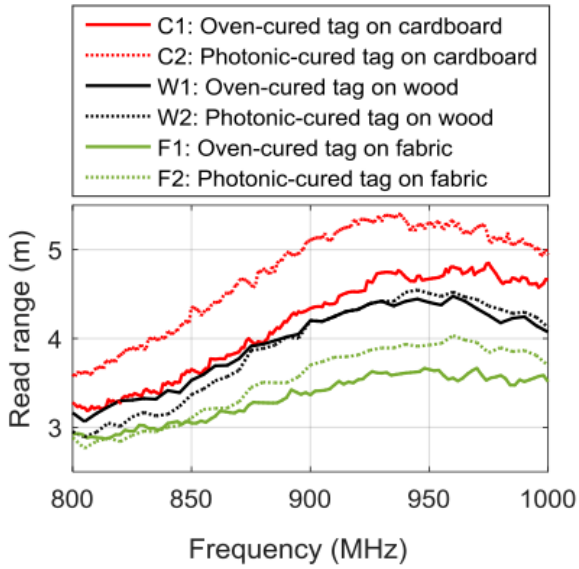

Figure 4.23: Read ranges of oven- and photonic-cured graphene tags on cardboard (C1, C2), wood (W1, W2), and fabric (F1, F2). **(Publication VIII)**

In general, the tags on cardboard cover longest read ranges, compared to tags on textile and wood substrates. This difference is as a result of difference in properties of the substrate materials, ink spreading and wetting on the substrate, and ink absorption into the substrate. It should be considered that low HV value and pulse numbers were utilized for the antennas on fabric and wood due to photonic curing limitations (Table 4.5).

The outcomes achieved in this study present the effectiveness of photonic curing technique as an alternative for conventional heating in the printed graphene structures.

5 Conclusion

The thesis studied different manufacturing methods for patterning graphene inks on versatile substrates. The resulting patterned graphene laminate can be used in widespread applications. In **Publication I**, inkjet printing was used as the manufacturing method to print graphene oxide ink, which was then annealed and thermally reduced at flowing nitrogen or argon-hydrogen atmosphere to form RGO. The results indicate argon-hydrogen atmosphere assists to better reduction due to deeper penetration of small-sized hydrogen atoms into graphene oxide structure. The **Publication II** introduced the possibility of using pulsed Xenon flashes to photonically reduce GO. This is a chemical-free and fast process with the benefit of performing at low temperatures. However, the challenge was uncontrollable dimension changes during flash reduction. The mechanical durability can be enhanced by adding polystyrene nanoparticles into GO, resulting RGO/PS nanocomposite after flash reduction with improved mechanical properties. Furthermore, the sheet resistance decreased dramatically compared with thermally reduced GO.

In **Publications III-VIII**, extensive work was carried out on manufacturing of graphene-based passive UHF RFID tags on versatile substrates. The results were eco-friendly and cost-effective tags. Moreover, these tags were studied in accordance with materials and electrical characterization, and wireless performance. The **Publications III-VI** show tags manufactured by doctor-blade technique on flexible green substrates. Based on reliability tests, these graphene passive RFID tags show acceptable response and reliability, when subjected to harsh bending and high humidity condition. According to the results, the attainable read range values of graphene tags on fabrics were increased when subjected to 100 % high humidity level and returned back to normal read range after curing. Additionally, the attainable read range values of graphene tags on cardboards gradually decreased after bending cycles.

The results of **Publication VIII** indicate that integrating of 3D printing and photonic curing introduces rapid and economical way for graphene-based antenna production on green substrates. The photonic curing enhances the wireless performance compared to conventional oven curing.

This thesis mainly studied graphene-based passive RFID tags on versatile green substrates, introducing them as a good candidate for environmentally-friendly wireless platforms, as well as for wearable components. The results show that graphene is a cost-effective material with excellent processability. The results imply that these graphene passive RFID tags are suitable for small range tracking and environmental monitoring. Graphene has a great potential for using in wireless applications.

Future trend

Graphene is a novel nanomaterial with extraordinary properties. The important things that should be addressed in future work are to develop the graphene-based inks to be more suitable for different ink-based manufacturing methods. It is still required to focus more on the development of graphene inks with higher conductivity. The challenge is to keep the balance between desires to smooth printing process, and have higher conductivity and mechanical durability.

The other challenge is related to the stretching of these tags. After stretching, severe cracks occurred on the printed area, and had drastic effect on the tag performance.

Additionally, huge potential lies on the versatile and novel applications of these graphene RFIDs. The wireless elements can be optimized for different designs, substrates and applications. Especially, environmentally-friendly wireless sensing platforms and wearable applications are interesting future areas. In particular, graphene has a great potential for short-range tracking and sensing, can be utilized at the parcel or letter tracking.

Bibliography

Acik, M. and Chabal, Y. J., "A review on thermal exfoliation of graphene oxide," *Journal of Materials Science Research*, vol. 2, no. 1, pp. 101–109, Jan 2013.

AlexanderAIUS. (2014) (UCL wins £1m for clean hydrogen technology) kernel description. [Online]. Available: http://www.ucl.ac.uk/mathematical-physical-sciences/news-events/maps-news-publication/maps1403/. Accessed: 2017-05-14.

Andò, B., Baglio, S., Pasquale, G. D., Pollicino, A., D'Agata, S., Gugliuzzo, C., Lombardo, C., and Re, G., "An inkjet printed CO_2 gas sensor," *Procedia Engineering*, vol. 120, pp. 628–631, 2015.

Berni, A., Mennig, M., and Schmidt, H., *Doctor Blade*. Boston, MA: Springer US, 2004, pp. 89–92.

Björninen, T., Virkki, J., Sydänheimo, L., and Ukkonen, L., "Impact of recurrent stretching on the performance of electro-textile UHF RFID tags," in *Proceedings of the 5th Electronics System-integration Technology Conference (ESTC)*, Sept 2014, pp. 1–5.

Chen, W., Yan, L., and Bangal, P. R., "Preparation of graphene by the rapid and mild thermal reduction of graphene oxide induced by microwaves," *Carbon*, vol. 48, no. 4, pp. 1146–1152, 2010.

Cote, L. J., Cruz-Silva, R., and Huang, J., "Flash reduction and patterning of graphite oxide and its polymer composite," *Journal of the American Chemical Society*, vol. 131, no. 31, pp. 11 027–11 032, 2009, pMID: 19601624.

Dankoco, M., Tesfay, G., Benevent, E., and Bendahan, M., "Temperature sensor realized by inkjet printing process on flexible substrate," *Materials Science and Engineering: B*, vol. 205, pp. 1–5, 2016.

Das, S., Yang, B., Gu, G., Joshi, P. C., Ivanov, I. N., Rouleau, C. M., Aytug, T., Geohegan, D. B., and Xiao, K., "High-performance flexible perovskite solar cells by using a combination of ultrasonic spray-coating and low thermal budget photonic curing," *ACS Photonics*, vol. 2, no. 6, pp. 680–686, 2015.

Derbek, V.and Steger, C., Weiss, R., Preishuber-Pflügl, J., and Pistauer, M., "A UHF RFID measurement and evaluation test system," *Elektrotechnik & Informationstechnik*, vol. 124, no. 11, pp. 384–390, 2007.

Dobkin, D. M., "Chapter 3 - Radio Basics For UHF RFID," in *The RF in RFID*, Dobkin, D. M., Ed. Burlington: Newnes, 2008, pp. 51 – 101.

Farnsworth, S., Schroder, K., Wenz, B., Pope, D., and Rawson, I., "32.4: Invited paper: Broad implications arising from photonic curing process for printed electronics and displays," *SID Symposium Digest of Technical Papers*, vol. 43, no. 1, pp. 430–433, 2012.

Feng, J., Li, W., Qian, X., Qi, J., Qi, L., and Li, J., "Patterning of graphene," *Nanoscale*, vol. 4, pp. 4883–4899, 2012.

Finkenzeller, K., *RFID Handbook: Fundamentals and Applications in Contactless Smart Cards, Radio Frequency Identification*. Chichester, UK: Wiley, 2003.

Fu, Y. Y., Chan, Y. L., Yang, M. H., Chan, Y. C., Virkki, J., Björninen, T., Sydänheimo, L., and Ukkonen, L., "Experimental study on the washing durability of electro-textile UHF RFID tags," *IEEE Antennas and Wireless Propagation Letters*, vol. 14, pp. 466–469, 2015.

Gebhardt, B., "Type selective functionalization of single-walled carbon nanotubes," Ph.D. dissertation, Friedrich-Alexander-Universität Erlangen-Nürnberg, 5 2012.

Gibson, I., Rosen, D., and Stucker, B., *Additive Manufacturing Technologies: 3D Printing, Rapid Prototyping, and Direct Digital Manufacturing*. New York: Springer, 2015, Second Edition.

Graphene-flagship. (2016) Graphene enables fully flexible NFC antennas. [Online]. Available: https://graphene-flagship.eu/graphene-enables-fully-flexible-nfc-antennas. Accessed: 2017-05-10.

Grunwald, I., Groth, E., Wirth, I., Schumacher, J., Maiwald, M., Zoellmer, V., and Busse, M., "Surface biofunctionalization and production of miniaturized sensor structures using aerosol printing technologies," *Biofabrication*, vol. 2, no. 1, p. 014106, 2010.

Technical Data Sheet - HDPlas®IGSC02002, Screen Printable Graphene Ink, Haydale Limited., 2015.

Heyrovska, R., "Atomic structures of graphene, benzene and methane with bond lengths as sums of the single, double and resonance bond radii of carbon," pp. 1–4, 2008, Preprint arXiv:0804.4086.

Huang, X., Leng, T., Zhang, X., Chen, J. C., Chang, K. H., Geim, A. K., Novoselov, K. S., and Hu, Z., "Binder-free highly conductive graphene laminate for low cost printed radio frequency applications," *Applied Physics Letters*, vol. 106, no. 20, p. 203105, 2015.

Hunt, V. D., Puglia, A., and Puglia, M., *RFID-A Guide to Radio Frequency Identification*. Hoboken, NJ: Wiley, 2007.

Hösel, M., "Large-scale roll-to-roll fabrication of organic solar cells for energy production," Ph.D. dissertation, Technical University of Denmark, Denmark, 2013.

Jariwala, D., Sangwan, V. K., Lauhon, L. J., Marks, T. J., and Hersam, M. C., "Carbon nanomaterials for electronics, optoelectronics, photovoltaics, and sensing," *Chem. Soc. Rev.*, vol. 42, pp. 2824–2860, 2013.

Kang, X., Zuo, Q., Yuan, C., Wang, W., Gao, M., Jiang, L., Zhou, Y., Wang, Y., Chen, S., Zhao, Y., Liu, J., Sheng, W., and Zhou, J., "Humidity sensor with graphene oxide as sensing material," in *2015 IEEE 11th International Conference on ASIC (ASICON)*, Nov 2015, pp. 1–3.

Kim, H.-S., Dhage, S. R., Shim, D.-E., and Hahn, H. T., "Intense pulsed light sintering of copper nanoink for printed electronics," *Applied Physics A*, vol. 97, no. 4, p. 791, 2009.

Larciprete, R., Fabris, S., Sun, T., Lacovig, P., Baraldi, A., and Lizzit, S., "Dual path mechanism in the thermal reduction of graphene oxide," *Journal of the American Chemical Society*, vol. 133, no. 43, pp. 17 315–17 321, 2011.

Le, L. T., Ervin, M. H., Qiu, H., Fuchs, B. E., and Lee, W. Y., "Graphene supercapacitor electrodes fabricated by inkjet printing and thermal reduction of graphene oxide," *Electrochemistry Communications*, vol. 13, no. 4, pp. 355–358, 2011.

Lehtimäki, S., Pörhönen, J., Tuukkanen, S., Moilanen, P., Virtanen, J., and Lupo, D., "Fabrication and characterization of solution-processed carbon nanotube supercapacitors," *MRS Proceedings*, vol. 1659, pp. 113–118, 2014.

Lewis, J. A., "Direct-write assembly of ceramics from colloidal inks," *Current Opinion in Solid State and Materials Science*, vol. 6, no. 3, pp. 245–250, 2002.

Lewis, J. A. and Gratson, G. M., "Direct writing in three dimensions," *Materials Today*, vol. 7, no. 7–8, pp. 32–39, 2004.

Li, B., Roy, T. D., Smith, C. M., Clark, P. A., and Church, K. H., "A robust true direct-print technology for tissue engineering," in *ASME 2007 International Manufacturing Science and Engineering Conference*, October 2007, pp. 103–108.

Miorandi, D., Sicari, S., Pellegrini, F. D., and Chlamtac, I., "Internet of things: Vision, applications and research challenges," *Ad Hoc Networks*, vol. 10, no. 7, pp. 1497–1516, 2012.

Molitor, F., Güttinger, J., Stampfer, C., Dröscher, S., Jacobsen, A., Ihn, T., and Ensslin, K., "Electronic properties of graphene nanostructures," *Journal of Physics: Condensed Matter*, vol. 23, no. 24, p. 243201, 2011.

Mortara, L., Hughes, J., Ramsundar, P. S., Livesey, F., and Probert, D. R., "Proposed classification scheme for direct writing technologies," *Rapid Prototyping Journal*, vol. 15, no. 4, pp. 299–309, 2009.

Niittynen, J., "Comparison of sintering methods and conductive adhesives for interconnections in inkjet-printed flexible electronics," Ph.D. dissertation, Tampere University of Technology, 2015.

Specification Sheet - Smart Pump^{TM}, nScrypt Inc., 2016.

Palacios, T., Hsu, A., and Wang, H., "Applications of graphene devices in RF communications," *IEEE Communications Magazine*, vol. 48, no. 6, pp. 122–128, June 2010.

Panico, L. (2010) Mastering printed electronics principles: Photonic drying – pulsed light as a low temperature sintering process. [Online]. Available: http://www.xenoncorp.com/files/2113/9301/9194/XenonCorpPresentationOnInkDrying.pdf. Accessed: 2017-05-15.

Perelaer, J., de Laat, A. W. M., Hendriks, C. E., and Schubert, U. S., "Inkjet-printed silver tracks: low temperature curing and thermal stability investigation," *J. Mater. Chem.*, vol. 18, pp. 3209–3215, 2008.

Popov, A., Dudnikov, S., and Mikhaylov, A., "Passive UHF RFID tag with increased read range," in *2008 38th European Microwave Conference*, Oct 2008, pp. 1106–1108.

Savage, N. (2009) Graphene makes transistors tunable. [Online]. Available: http://spectrum.ieee.org/semiconductors/materials/graphene-makes-transistors-tunable.

Schedin, F., Geim, A. K., Morozov, S. V., Hill1, E. W., Blake1, P., Katsnelson, M. I., and Novoselov, K. S., "Detection of individual gas molecules adsorbed on graphene," *Journal of Physics: Condensed Matter*, vol. 6, pp. 652–655, 2007.

Schroder, K., "Mechanisms of photonic curing™: Processing high temperature films on low temperature substrates," vol. 2, 2011, pp. 220–223.

Schäffel, F., "Chapter 2 - the atomic structure of graphene and its few-layer counterparts," in *Graphene*, Warner, J. H., Schäffel, F., Bachmatiuk, A., and Rümmeli, M. H., Eds. Elsevier, 2013, pp. 5–59.

Shen, H., Zhang, L., Liu, M., and Zhang, Z., "Biomedical applications of graphene," *Theranostics*, vol. 2, no. 3, p. 283–294, 2012.

Singh, M., Haverinen, H. M., Dhagat, P., and Jabbour, G. E., "Inkjet printing—process and its applications," *Advanced Materials*, vol. 22, no. 6, pp. 673–685, 2010.

Sipilä, E., Virkki, J., Sydänheimo, L., and Ukkonen, L., "Effect of sintering method on the read range of brush-painted silver nanoparticle UHF RFID tags on wood and polyimide substrates," in *2014 IEEE RFID Technology and Applications Conference (RFID-TA)*, Sept 2014, pp. 219–222.

Sipilä, E., "Novel manufacturing methods and materials for UHF RFID tags in identification and sensing applications," Ph.D. dissertation, Tampere University of Technology, 2016.

Smith, A. D., Elgammal, K., Niklaus, F., Delin, A., Fischer, A. C., Vaziri, S., Forsberg, F., Rasander, M., Hugosson, H., Bergqvist, L., Schroder, S., Kataria, S., Ostling, M., and Lemme, M. C., "Resistive graphene humidity sensors with rapid and direct electrical readout," *Nanoscale*, vol. 7, pp. 19 099–19 109, 2015.

Sowade, E., Ramon, E., Mitra, K. Y., Martínez-Domingo, C., Pedró, M., Pallarès, J., Loffredo, F., Villani, F., Gomes, H. L., Terés, L., and Baumann, R. R., "All-inkjet-printed thin-film transistors: manufacturing process reliability by root cause analysis," *Scientific Reports*, vol. 6, no. 33490, pp. 1–15, 2016.

Stoppa, M. and Chiolerio, A., "Wearable electronics and smart textiles: A critical review," *Sensors*, vol. 14, no. 7, pp. 11 957–11 992, 2014.

Therriault, D., White, S. R., and Lewis, J. A., "Chaotic mixing in three-dimensional microvascular networks fabricated by direct-write assembly," *Nature Materials*, vol. 2, pp. 265–271, 2003.

Varma, V., Scheffer, D., Ginneman, C., and Lettow, J., "Polymeric compositions containing graphene sheets and graphite," Jun 2012, US Patent App. 13/260,372.

Virkki, J., Björninen, T., Merilampi, S., Sydänheimo, L., and Ukkonen, L., "The effects of recurrent stretching on the performance of electro-textile and screen-printed ultra-high-frequency radio-frequency identification tags," *Textile Research Journal*, vol. 85, no. 3, pp. 294–301, 2015.

Voit, W., Zapka, W., Belova, L., and Rao, K. V., "Application of inkjet technology for the deposition of magnetic nanoparticles to form micron-scale structures," *IEE Proceedings - Science, Measurement and Technology*, vol. 150, no. 5, pp. 252 – 256, Sept 2003.

Voyantic. (2017) Tagformance lite. [Online]. Available: http://voyantic.com/products/tagformance-lite. Accessed: 2017-05-12.

Vuorinen, T., Niittynen, J., Kankkunen, T., Kraft, T. M., and Mäntysalo, M., "Inkjet-printed graphene/pedot:pss temperature sensors on a skin-conformable polyurethane substrate," *Scientific Reports*, vol. 6, no. 35289, pp. 1 – 8, 2016.

Want, R., "An introduction to rfid technology," *IEEE Pervasive Computing*, vol. 5, no. 1, pp. 25 – 33, Jan 2006.

Wengeler, L., Schmitt, M., Peters, K., Scharfer, P., and Schabel, W., "Comparison of large scale coating techniques for organic and hybrid films in polymer based solar cells," *Chemical Engineering and Processing: Process Intensification*, vol. 68, pp. 38 – 44, 2013, advances in Coating and Drying of Thin Films.

Xenon-Corporation, *Xenon Sinteron 2010-L*, June 2013.

Xu, J., Wang, Y., Shan, H., Lin, Y., Chen, Q., Roy, V. A. L., and Xu, Z., "Ultrasound-induced organogel formation followed by thin film fabrication via simple doctor blading technique for field-effect transistor applications," *ACS Applied Materials & Interfaces*, vol. 8, no. 29, pp. 18 991 – 18 997, 2016, PMID: 27377991.

Yavari, F., Castillo, E., Gullapalli, H., Ajayan, P. M., and Koratkar, N., "High sensitivity detection of NO_2 and NH_3 in air using chemical vapor deposition grown graphene," *Applied Physics Letters*, vol. 100, no. 20, p. 2031202, 2012.

Zakaryan, H. and Aroutionian, V., "Sensitivity of graphene humidity sensors," in *AMA Conferences 2015-Proceedings SENSOR 2015*, May 2015, pp. 868 – 872.

Zhang, B., Wang, Y., and Zhai, G., "Biomedical applications of the graphene-based materials," *Materials Science and Engineering: C*, vol. 61, pp. 953 – 964, 2016.

Zheng, Q., Lu, J., Chen, H., Huang, L., Cai, J., and Xu, Z., "Application of inkjet printing technique for biological material delivery and antimicrobial assays," *Analytical Biochemistry*, vol. 410, no. 2, pp. 171 – 176, 2011.

Tampereen teknillinen yliopisto
PL 527
33101 Tampere

Tampere University of Technology
P.O.B. 527
FI-33101 Tampere, Finland

ISBN 978-952-15-4006-6
ISSN 1459-2045